The Journal of Chemical Physics

A two-layer approach to the coupled coherent states method

Cite as: J. Chem. Phys. **144**, 024111 (2016); https://doi.org/10.1063/1.4939205
Submitted: 01 July 2015 • Accepted: 17 December 2015 • Published Online: 12 January 2016

James A. Green, Adriano Grigolo, Miklos Ronto, et al.

A two-layer approach to the coupled coherent states method

James A. Green,[1,a)] Adriano Grigolo,[2,b)] Miklos Ronto,[1,c)] and Dmitrii V. Shalashilin[1,d)]
[1]*School of Chemistry, University of Leeds, Leeds LS2 9JT, United Kingdom*
[2]*Instituto de Física "Gleb Wataghin," Universidade Estadual de Campinas, 13083-859 Campinas, SP, Brazil*

(Received 1 July 2015; accepted 17 December 2015; published online 12 January 2016)

In this paper, a two-layer scheme is outlined for the coupled coherent states (CCS) method, dubbed two-layer CCS (2L-CCS). The theoretical framework is motivated by that of the multiconfigurational Ehrenfest method, where different dynamical descriptions are used for different subsystems of a quantum mechanical system. This leads to a flexible representation of the wavefunction, making the method particularly suited to the study of composite systems. It was tested on a 20-dimensional asymmetric system-bath tunnelling problem, with results compared to a benchmark calculation, as well as existing CCS, matching-pursuit/split-operator Fourier transform, and configuration interaction expansion methods. The two-layer method was found to lead to improved short and long term propagation over standard CCS, alongside improved numerical efficiency and parallel scalability. These promising results provide impetus for future development of the method for on-the-fly direct dynamics calculations. [http://dx.doi.org/10.1063/1.4939205]

I. INTRODUCTION

Multilayer variants of existing numerical methods in multidimensional quantum mechanics offer an increase in flexibility and give better scalability for the description of complex quantum systems. Motivated by the extension of multiconfigurational time-dependent Hartree (MCTDH)[1,2] to its multilayer formalism (ML-MCTDH),[3–5] Gaussian based methods have already been extended in this direction, and a two-layer approach for the Gaussian-based MCTDH (G-MCTDH) has been proposed in Ref. 6.

Numerous Gaussian based techniques exist for both semiclassical and quantum propagations. Following the seminal work by Heller,[7] many of those methods represent the wavefunction as a superposition of trajectory guided Gaussian coherent states,

$$|\Psi(t)\rangle = \sum_{n=1}^{N} A_n(t)|\mathbf{z}_n(t)\rangle. \tag{1}$$

In the z-notation representation of coherent states, an M-dimensional coherent state (CS) is a product of M one-dimensional Gaussian wavepackets: $|\mathbf{z}\rangle = \prod_{i=1}^{M} |z^{(i)}\rangle$. The position representation of these states is

$$\langle x|z^{(i)}\rangle = (\gamma/\pi)^{\frac{1}{4}} e^{-\frac{\gamma}{2}(x-q^{(i)})^2 + \frac{i}{\hbar}p^{(i)}(x-q^{(i)}) + \frac{i}{2\hbar}p^{(i)}q^{(i)}}, \tag{2}$$

where γ describes the width of the Gaussian and $q^{(i)}$ and $p^{(i)}$ are the coordinate and momentum in the ith dimension. These phase space coordinates are related to the real and imaginary parts of the CS label,

$$z = \sqrt{\frac{\gamma}{2}}q + \frac{i}{\hbar}\sqrt{\frac{1}{2\gamma}}p, \tag{3}$$

which is motivated by the fact that $|z\rangle$ and z are the eigenvector and eigenvalue of the annihilation operator, respectively,

$$\hat{a}|z\rangle = z|z\rangle; \qquad \hat{a} = \sqrt{\frac{\gamma}{2}}\hat{q} + \frac{i}{\hbar}\sqrt{\frac{1}{2\gamma}}\hat{p}. \tag{4}$$

The amplitudes in Eq. (1) are usually represented as a product of an oscillating action exponent and smooth pre-exponential factor,[8]

$$A_n(t) = D_n(t)e^{\frac{i}{\hbar}S_n(t)}. \tag{5}$$

Several methods exist for guiding the trajectories of the CS basis. Semiclassical methods such as Heller's frozen Gaussian approximation[7] and the Herman-Kluk propagator[9–11] use classical trajectories and a semiclassical description for the amplitudes. There are also a number of formally exact Gaussian-based methods such as multiple spawning (MS),[12,13] coupled coherent states (CCS),[8,14–16] and variational multiconfigurational Gaussians (vMCG).[17,18] These methods use exact quantum equations for the amplitudes $A_n(t)$ in Eq. (1) but differ in the way that the basis $|\mathbf{z}_n(t)\rangle$ is guided. MS uses purely classical mechanics whereas vMCG relies on complicated trajectories obtained from a full variational principle applied to the complete wavefunction $|\Psi(t)\rangle$. The fully variational trajectories of vMCG are strongly quantum: different basis vectors $\mathbf{z}_n(t)$ couple to one another as well as with their amplitudes. CCS can be placed between the two approaches, relying on classical trajectories with simple quantum corrections. Trajectory based quantum techniques are reminiscent of classical molecular dynamics (MD) and are capable of representing quantum molecular dynamics.

a)Electronic mail: cmjg@leeds.ac.uk
b)Electronic mail: agrigolo@ifi.unicamp.br
c)Electronic mail: m.ronto@leeds.ac.uk
d)Electronic mail: d.shalashilin@leeds.ac.uk

The main advantage of trajectory guided methods is that most of the time the basis set follows the dynamically important region, thus economising its size. However, in many cases, a small trajectory guided basis is efficient for short time period only. When trajectories in multidimensional phase space run away from each other, even fully variational trajectories become uncoupled and classical. Therefore, they become unable to correctly follow the dynamics in strongly non-classical degrees of freedom (DOF), misguiding the basis. To address this issue, the multiconfigurational Ehrenfest (MCE)[19,20] approach was suggested. In the version of MCE proposed in Ref. 20, a regular basis set is used to represent the dynamics in a "more quantum" subsystem instead of a single CS. The Ehrenfest configuration basis takes the form

$$|\varphi_n(t)\rangle = (a_{1n}(t)|1\rangle + a_{2n}(t)|2\rangle + \cdots + a_{Kn}(t)|K\rangle)\,|\mathbf{z}_n^{(c)}(t)\rangle, \tag{6}$$

where the set of states $\{|1\rangle,|2\rangle,\ldots,|K\rangle\}$ represents an orthonormal basis of K functions for the "quantum" subsystem, for example, K electronic potential energy surfaces like in Ref. 20 or a set of K discrete value representation (DVR) points. A single Gaussian trajectory guided coherent state, $|\mathbf{z}_n^{(c)}(t)\rangle$, describes the "classical" degrees of freedom. A single Ehrenfest configuration is not flexible enough to describe complicated quantum dynamics accurately but a superposition of Ehrenfest configurations

$$|\Psi(t)\rangle = \sum_{n=1}^{N} A_n(t)|\varphi_n(t)\rangle, \tag{7}$$

can be converged to a quantum result. As Eq. (7) represents the whole wavefunction as a superposition of Ehrenfest configurations, even "classical" degrees of freedom are represented on a fully quantum level irrespective of the fact that within a given configuration, such as in Eq. (6), they are described by a single CS. Coupling between the coefficients $A_n(t)$ in Eq. (7) ensures that the trajectories $|\mathbf{z}_n^{(c)}(t)\rangle$ are weighted according to quantum dynamics. Several versions of MCE exist, and results have been obtained for spin-boson model,[19] non-adiabatic dynamics of pyrazine,[20] dynamics of adsorption on the surface,[21] and dynamics of quantum qubits coupled with the electromagnetic field.[22] G-MCTDH[23] method also relies on the same idea of using regular MCTDH wavefunctions for a small "quantum" subsystem and Gaussian wavepackets for "classical" degrees of freedom.

In this paper, we suggest a variation of MCE, which—instead of a regular basis—uses Gaussian CSs for the "quantum" subsystem. The algorithm, which is termed as two-layer CCS (2L-CCS), is fully trajectory based and represents quantum molecular dynamics. Many quantum techniques, which use the basis of trajectory guided Gaussian CS, have been implemented in Cartesian frame (Cartesian CCS,[24] MS,[12,13] MCE,[25–28] vMCG[17,18] on-the-fly) so that they would work similar to classical MD. A great deal of effort has been invested in the development of quantum direct dynamics, which uses electronic structure software packages on-the-fly to estimate forces which in turn guide the trajectories and the matrix elements of quantum coupling between them.[12,13,25–28] So far these direct dynamics methods have been focused on electronically non-adiabatic effects. Being a trajectory based method, 2L-CCS is well suited to Cartesian frame implementation, and we point out from the outset that the future aim is to implement 2L-CCS in this manner so that it may provide a better description of tunnelling in *ab initio* direct dynamics simulations than standard CCS. Throughout the remainder of the paper, atomic units are used with $\hbar = 1$, and the coherent state parameter γ in Eq. (2) is set to unity.

II. WORKING EQUATIONS OF TWO-LAYER CCS

A. Wavefunction ansatz

Assuming that the system is comprised of "quantum" and "classical" subsystems, we represent the Ehrenfest configuration[29–31] as follows:

$$|\varphi_n(t)\rangle = \Big(a_{1n}(t)|\mathbf{z}_{1n}^{(q)}(t)\rangle + a_{2n}(t)|\mathbf{z}_{2n}^{(q)}(t)\rangle + \cdots + a_{Kn}(t)|\mathbf{z}_{Kn}^{(q)}(t)\rangle\Big)\,|\mathbf{z}_n^{(c)}(t)\rangle. \tag{8}$$

In this equation, $|\mathbf{z}_{kn}^{(q)}\rangle = \prod_{i=1}^{M^{(q)}}|z_{kn}^{(i)}\rangle$ and $|\mathbf{z}_n^{(c)}\rangle = \prod_{i=M^{(q)}+1}^{M}|z_n^{(i)}\rangle$ are the coherent states covering $M^{(q)}$ "quantum" and the remaining "classical" degrees of freedom. The difference between Eqs. (6) and (8) is that in the latter, the "quantum" subsystem is represented not on a regular fixed basis set but on the basis of trajectory guided CSs. The "classical" subsystem is still represented by a single Gaussian. The total wavefunction is a superposition of configurations,

$$|\Psi(t)\rangle = \sum_{n=1}^{N} D_n(t)|\varphi_n(t)\rangle \tag{9a}$$

$$= \sum_{n=1}^{N} D_n(t)\left[\sum_{k=1}^{K} a_{kn}(t)|\mathbf{z}_{kn}^{(q)}\rangle\right]|\mathbf{z}_n^{(c)}(t)\rangle \tag{9b}$$

$$= \sum_{n=1}^{N} D_n(t)\left[\sum_{k=1}^{K} a_{kn}(t)|\mathbf{z}_{kn}(t)\rangle\right]. \tag{9c}$$

In Eq. (9), N is the number of configurations and K is the number of Gaussian CSs $|\mathbf{z}_{kn}^{(q)}\rangle$ describing the "quantum" subsystem in a single configuration. Therefore, even the "classical" subsystem is treated on a fully quantum level and the ansatz of Eq. (9) is formally exact: it can be converged (at least in principle) to the fully quantum result. It is convenient to introduce full dimensional CS,

$$|\mathbf{z}_{kn}(t)\rangle = |\mathbf{z}_{kn}^{(q)}(t)\rangle|\mathbf{z}_n^{(c)}(t)\rangle \tag{10}$$

as in Eq. (9c), bearing in mind that for a given index n, all $|\mathbf{z}_{kn}(t)\rangle$ with different k differ only by their "quantum" part.

Coherent states are not orthogonal: the overlap between two states is described by the overlap matrix,[32]

$$\langle\mathbf{z}_{kn}|\mathbf{z}_{lm}\rangle = \exp\left[\mathbf{z}_{kn}^{*}\mathbf{z}_{lm} - \frac{\mathbf{z}_{kn}^{*}\mathbf{z}_{kn}}{2} - \frac{\mathbf{z}_{lm}^{*}\mathbf{z}_{lm}}{2}\right]. \tag{11}$$

The matrix elements of the Hamiltonian can be written in coherent state basis by representing the Hamiltonian with creation and annihilation operators in normal order (powers of the creation operator to the left of those of the annihilation operator); the matrix elements become

$$\langle\mathbf{z}_{kn}|\hat{H}|\mathbf{z}_{lm}\rangle = \langle\mathbf{z}_{kn}|\mathbf{z}_{lm}\rangle H_{ord}(\mathbf{z}_{kn}^{*},\mathbf{z}_{lm}), \tag{12}$$

where in the normal ordered Hamiltonian $H_{ord}(\hat{a}^\dagger, \hat{a})$, $\hat{a}^\dagger$ and $\hat{a}$ are simply replaced by z^* and z, respectively.

B. Equations of motion

Time-dependence of the phase space coordinates of the CSs $|\mathbf{z}_{kn}^{(\mathrm{q})}\rangle$ and $|\mathbf{z}_{n}^{(\mathrm{c})}\rangle$, as well as their corresponding amplitudes $a_{kn}(t)$ and $D_n(t)$, determines the time-evolution of the wavefunction. The equations of motion can be obtained from a full variational approach by taking (9) as a trial state and optimising all wavefunction parameters $\{\mathbf{z}_{kn}^{(\mathrm{q})}, \mathbf{z}_{n}^{(\mathrm{c})}, a_{kn}, D_n\}$ at once. This procedure has been applied to Gaussian based wavefunctions in Refs. 6, 18, 23, and 33; however, one can also treat some of the parameters variationally while prescribing the dynamics of the others. Under this scheme, different methods can be used within a single configuration to propagate the "quantum" and "classical" sub-systems. In this work, we use predetermined CCS and Ehrenfest type trajectories for z_{kn} and z_n, respectively, which intuitively follows from our experience with each method. This is combined with variational equations for the amplitudes in each layer which ensures that 2L-CCS is an (in principle) exact technique. It is important to point out that the prescribed CS dynamics is not an approximation, but rather a convenient, simple, and stable way of guiding the basis set. Providing the basis set sufficiently covers phase space over the time frame of a calculation, the exact result may be obtained. See, for example, Ref. 34 where the efficiency of guiding the basis by classical and variational trajectories is compared, and both are shown to converge to the same result. The particular prescriptions employed here find their justification in the time-dependent variational principle (TDVP) when it is applied to individual basis set elements and configurations. The derivation of the working equations, which involves using normalisation constraints and appropriate choice of phases for the CS elements, is presented separately in Appendix A.

In the first layer, the standard CCS basis equation,

$$\dot{\mathbf{z}}_{kn}^{(\mathrm{q})} = -i\frac{\partial H_{ord}(\mathbf{z}_{kn}^{*}\mathbf{z}_{kn})}{\partial \mathbf{z}_{kn}^{(q)*}}, \tag{13}$$

is used to describe the dynamics of "quantum" coordinates. As has been discussed in Refs. 8, 14, and 15, trajectories (13) are classical in nature, although the Hamiltonian includes quantum corrections. The amplitudes are conveniently written as a product of an oscillating action exponent and smooth pre-exponential factor

$$a_{kn} = d_{kn}e^{iS_{kn}}, \tag{14}$$

with classical action

$$S_{kn} = \int_0^t \left[\frac{i}{2}(\mathbf{z}_{kn}^{*}\dot{\mathbf{z}}_{kn} - \dot{\mathbf{z}}_{kn}^{*}\mathbf{z}_{kn}) - H_{ord}(\mathbf{z}_{kn}^{*}, \mathbf{z}_{kn})\right] dt'. \tag{15}$$

The equations of motion for d can be found as

$$i\sum_{l=1}^{K}\langle \mathbf{z}_{kn}|\mathbf{z}_{ln}\rangle \dot{d}_{ln}e^{iS_{ln}} = \sum_{l=1}^{K}\langle \mathbf{z}_{kn}|\mathbf{z}_{ln}\rangle \delta^2 H'_{kn,ln} d_{ln}e^{iS_{ln}}, \tag{16}$$

where

$$\delta^2 H'_{kn,ln} = H_{ord}(\mathbf{z}_{kn}^{*}, \mathbf{z}_{ln}) - H_{ord}(\mathbf{z}_{ln}^{*}, \mathbf{z}_{ln}) - i(\mathbf{z}_{kn}^{*} - \mathbf{z}_{ln}^{*})\dot{\mathbf{z}}_{ln}. \tag{17}$$

This is the same as in the CCS method, the only difference being that the Hamiltonian matrix elements have explicit time-dependence due to the motion of "classical" modes. Equations (13), (15), and (16) constitute the first layer of the two-layer CCS approach.

For the second layer of "classical" degrees of freedom, MCE equations are used for the trajectories,

$$\dot{\mathbf{z}}_{n}^{(\mathrm{c})} = -i\frac{\partial\langle\varphi_n|\hat{H}|\varphi_n\rangle}{\partial \mathbf{z}_{n}^{(c)*}} \tag{18a}$$

$$= -i\sum_{kl=1}^{K} d_{kn}^{*}d_{ln}\langle \mathbf{z}_{kn}^{(\mathrm{q})}|\mathbf{z}_{ln}^{(\mathrm{q})}\rangle \frac{\partial H_{ord}(\mathbf{z}_{kn}^{*}\mathbf{z}_{ln})}{\partial \mathbf{z}_{n}^{(c)*}} e^{i(S_{ln}-S_{kn})}. \tag{18b}$$

Ehrenfest trajectories (18) account for the effect of the "quantum" subsystem on the motion of the "classical" subsystem by averaging the Hamiltonian of classical DOF with the wavefunction of "quantum" subsystem. The "classical" DOF Hamiltonian itself also includes CCS quantum corrections. Then, upon substitution of the resulting wavefunction in the time-dependent Schrödinger equation, the equations for the amplitudes of configurations are found to be

$$i\sum_{m=1}^{N}\langle\varphi_n|\varphi_m\rangle\dot{D}_m = \sum_{m=1}^{N}\left[\langle\varphi_n|\hat{H}|\varphi_m\rangle - i\langle\varphi_n|\dot{\varphi}_m\rangle\right]D_m, \tag{19}$$

which can be recast in terms of the basic variables as

$$i\sum_{m=1}^{N}\sum_{kl=1}^{K} d_{kn}^{*}d_{lm}\langle \mathbf{z}_{kn}|\mathbf{z}_{lm}\rangle\dot{D}_m e^{i(S_{lm}-S_{kn})} = \sum_{m=1}^{N}\sum_{kl=1}^{K}\langle \mathbf{z}_{kn}|\mathbf{z}_{lm}\rangle d_{kn}^{*}\left(-i\dot{d}_{lm} + \Delta^2 H'_{kn,lm}d_{lm}\right)D_m e^{i(S_{lm}-S_{kn})}, \tag{20}$$

with the coupling matrix $\Delta^2 H'$ being

$$\Delta^2 H'_{kn,lm} = H_{ord}(\mathbf{z}_{kn}^{*}, \mathbf{z}_{lm}) - H_{ord}(\mathbf{z}_{lm}^{*}, \mathbf{z}_{lm}) - i(\mathbf{z}_{kn}^{*} - \mathbf{z}_{lm}^{*})\dot{\mathbf{z}}_{lm}. \tag{21}$$

Thus, the Ehrenfest equations of motion in Eqs. (18) and (20) are used for the trajectories and amplitudes of the "classical" layer. We again emphasise that even the second layer "classical" subsystem is treated on a fully quantum level. The only difference between "classical" and "quantum" layers is that the "classical" system is represented by a single

Gaussian and single trajectory per configuration, while the "quantum" subsystem is represented by a more flexible linear combination of K Gaussians per configuration guided by their individual trajectories. Similar to the CCS technique, the right hand side of coupled equations (16) and (20) is small. As has been shown previously (see Refs. 8, 14–16, and 18), matrices $\delta^2 H'$ and $\Delta^2 H'$ are small, sparse and have zero diagonal.

It should be noted that the two-layer equations of motion can be simplified by using the fact that $\langle \mathbf{z}_{kn}|\mathbf{z}_{ln}\rangle = \langle \mathbf{z}^{(q)}_{kn}|\mathbf{z}^{(q)}_{ln}\rangle$ and by splitting action (15) into two parts, one depending on both indices kn and the other depending only on the configuration index n—see Appendix A.

In this section, we have described another approach to guide the trajectories of a Gaussian CS basis set. Within a single configuration n, a small set of "quantum" DOF should be sampled with coherent states $\mathbf{z}^{(q)}_{kn}$ such that all important parts of the phase space of the "quantum" subsystem are covered. Using several CSs per configuration to parametrise the "quantum" subsystem describes quantum delocalisation better. The trajectories of "quantum" subsystem are given by CCS equation (13) and quantum effects are taken into account via the coupling of their amplitudes (16). The "classical" DOF is described by a single trajectory, which is influenced by the "quantum" subsystem via Ehrenfest equation (18). The description of "classical" DOF is less detailed. To account properly for quantum dynamics of the "classical" subsystem, the configurations are weighted with their amplitudes (19) and equations for the coupling coefficients are derived. The specific choice of trajectories (13) and (18), which are almost as simple and computationally inexpensive as classical trajectories, ensures the smallness and sparsity of the quantum coupling matrices in Eqs. (16) and (20). In summary, Eqs. (13), (16), (18), and (20) constitute the proposed 2L-CCS approach. If only one CS is used to describe the "quantum" subsystem ($k = 1$ in Eq. (9b)), then 2L-CCS yields the standard CCS method.

III. IMPLEMENTATION AND RESULTS

A. Hamiltonian

The test system investigated is that of a particle subjected to an asymmetric double well potential whose motion is also coupled to a bath; this same system was studied by the matching-pursuit/split-operator Fourier transform (MP/SOFT) method,[35] CCS,[36] and recently by a trajectory-guided strategy using a configuration interaction (CI) expansion of the wavefunction.[37] The model Hamiltonian

$$\hat{H} = \frac{\hat{p}^{(1)^2}}{2} - \frac{\hat{q}^{(1)^2}}{2} + \frac{\hat{q}^{(1)^4}}{16\xi} + \frac{\hat{\mathbf{P}}^2}{2} + \frac{\left(1 + \lambda \hat{q}^{(1)}\right)\hat{\mathbf{Q}}^2}{2} \tag{22}$$

is M-dimensional, where $(\hat{p}^{(1)}, \hat{q}^{(1)})$ are the position and momentum operators of the 1D tunnelling ("quantum") subspace and $(\hat{\mathbf{Q}}, \hat{\mathbf{P}})$ are the position and momentum operators of the $(M-1)$-dimensional ("classical") subspace, with $\hat{\mathbf{Q}} = \sum_{i=2}^{M} \hat{q}^{(i)}$ and $\hat{\mathbf{P}} = \sum_{i=2}^{M} \hat{p}^{(i)}$. As in previous works,[35–37] we consider the case of $M = 20$ and set the potential parameter $\xi = 1.3544$ and the system-bath coupling constant $\lambda = 0.1$. As the coupling is linear with respect to $q^{(1)}$ and quadratic with respect to $\mathbf{Q}$, the model describes the case of asymmetric tunnelling, because the coupling with the bath increases the right hand well depth for $q^{(1)} < 0$ and decreases it for $q^{(1)} > 0$. For the initial state, all bath modes are in their harmonic ground states.

For illustrative purposes, we also show the equations of motion used in 2L-CCS. If we denote $z^{(q)}_{kn} = (q^{(1)}_{kn} + ip^{(1)}_{kn})/\sqrt{2}$ and $\mathbf{z}^{(c)}_{n} = (\mathbf{Q}_n + i\mathbf{P}_n)/\sqrt{2}$, then the equations for the "quantum" modes read

$$\dot{q}^{(1)}_{kn} = p^{(1)}_{kn}, \tag{23a}$$

$$\dot{p}^{(1)}_{kn} = -\frac{(M-1)\lambda}{4} - \left(\frac{3}{8\xi} - 1\right) - \frac{q^{(1)^3}_{kn}}{4\xi} - \frac{\lambda}{2}\mathbf{Q}^2_n, \tag{23b}$$

while the "classical" modes are governed by

$$\dot{\mathbf{Q}}_n = \mathbf{P}_n, \tag{24a}$$

$$\dot{\mathbf{P}}_n = -\mathbf{Q}_n - \lambda\langle\varphi_n|\hat{q}^{(1)}|\varphi_n\rangle\mathbf{Q}_n, \tag{24b}$$

with $k = 1, 2, \ldots, K$ and $n = 1, 2, \ldots, N$. Equations (23) and (24) are different from those of classical mechanics. Most importantly, in the two-layer context, the "classical" modes couple with the "quantum" subsystem via the average value of the "quantum" mode position operator $\hat{q}^{(1)}$ over the nth configuration $|\varphi_n\rangle$; this average is explicitly given by

$$\langle\varphi_n|\hat{q}^{(1)}|\varphi_n\rangle = \sum_{kl=1}^{K} d^*_{kn} d_{ln} \langle z^{(q)}_{kn}|z^{(q)}_{ln}\rangle \left(\frac{z^{*(q)}_{kn} + z^{(q)}_{ln}}{\sqrt{2}}\right) e^{i(S^{(q)}_{ln} - S^{(q)}_{kn})}. \tag{25}$$

Clearly, the "quantum" nature of the 1D tunnelling mode makes itself present in the equations of motion for the "classical" (bath) coordinates. This clarifies the fundamental idea behind the two-layer approach: by taking into account this distinction between the different degrees of freedom at the level of the equations of motion for the "classical" (bath) modes, one hopes to enhance the quality of the configurations $|\varphi_n\rangle$ used to expand the system wavefunction as in (9), in the sense that the number of configurations needed to converge the results is expected to be minimised.

B. Benchmark calculation

The benchmark calculation relies on the fact that the modes $(\hat{\mathbf{Q}}, \hat{\mathbf{P}})$ are equivalent and thus effectively indistinguishable. As a result, one may use permutational symmetry and combine the multidimensional basis functions in groups. The approach is equivalent to second quantization and further details may be found in Appendix B or Ref. 38 which also contains full results for model Hamiltonian (22). The benchmark calculations are fully converged for the set of parameters used in this article for Hamiltonian (22).

C. Initial basis set sampling for CCS and 2L-CCS

In a multidimensional system, only a basis which is sufficiently compressed and biased to the position of the initial wavefunction $|\Psi(0)\rangle$ in phase space can result in an accurate representation. For Hamiltonian (22) considered in this work,

the initial wavefunction $|\Psi(0)\rangle$ is a multidimensional Gaussian wavepacket with phase space coordinates of the tunnelling mode located at the minimum of the lower well: $q^{(1)}(0) = -2.5$ and $p^{(1)}(0) = 0.0$, whilst initial coordinates of the bath mode are $q^{(i)}(0) = 0.0$ and $p^{(i)}(0) = 0.0$ for $i > 1$. As has been shown in Ref. 16, the quality of the initial basis can be assessed from the norm of the wavefunction. For a good quality basis, covering densely the phase space region where the whole wavefunction is located, the norm

$$\begin{aligned}\langle\Psi|\Psi\rangle &= \sum_{nm=1}^{N} D_n^*\langle\varphi_n|\varphi_m\rangle D_m \\ &= \sum_{nm=1}^{N} D_n^* D_m \sum_{kl=1}^{K} d_{kn}^* d_{lm} e^{i(S_{kn}-S_{lm})}\langle\mathbf{z}_{lm}|\mathbf{z}_{kn}\rangle \end{aligned} \quad (26)$$

becomes close to unity.

For the CCS method, initial random basis set sampling of the tunnelling mode and bath modes is centered around the initial tunnelling and bath positions, respectively, and conducted via a Monte Carlo distribution of the form[8]

$$f(z^{(i)}) \propto \exp(-\alpha^{(i)}|z^{(i)} - z^{(i)}(0)|^2). \quad (27)$$

The compression parameter $\alpha^{(i)}$ sets the width of the distribution in the ith degree of freedom; the larger the value of $\alpha^{(i)}$, the more compressed the distribution (this is merely a sampling parameter and is not connected to the width γ of the coherent state). Different initial basis set distributions can be used for different types of modes, in this case the tunnelling and bath modes. This is called a "pancake" distribution.[16] Sampling for 2L-CCS may proceed in exactly the same way as CCS, due to wavefunction ansatz (9) conveniently splitting the basis into "quantum" and "classical" subsystems, allowing "pancake" sampling.

In Ref. 36, for tunnelling problem (22), a broad distribution was used for the tunnelling ("quantum") mode and narrow distributions were used for the 19 bath ("classical") modes. However, the result obtained in that work was in some disagreement to that obtained by other methods.[35,37] Based on the sampling of MP/SOFT and CI expansion, and results from the benchmark calculation,[38] it was established that one of the possible reasons for this is that the bath was insufficiently sampled and a broader distribution is required. Consequently, the CCS calculation will be repeated in this work. However, it is not possible to sample all bath modes from a broad distribution, as this results in CSs that are inadequately coupled. Therefore, drawing on inspiration from the benchmark calculation in which a number of individual bath modes are "excited," a random two bath modes per configuration are sampled from a broad distribution ("excited") with compression parameter α^{b}, whilst all others are sampled with an infinite compression parameter. Both distributions are centred on the initial bath coordinates $q^{(i)}(0) = 0.0$ and $p^{(i)}(0) = 0.0$ for $i > 1$. This allows the value of α^{b} to be smaller than if all bath modes had the same compression parameter, permitting a greater range of phase space to be sampled. Choosing two modes to be decompressed rather than any other number was found to lead to an appropriate balance of ample bath sampling and well conserved norm near unity, though we admit this is quite an *ad hoc* approach which is left to be better understood in future investigation. The bath for both CCS and 2L-CCS is sampled in this way.

TABLE I. Sampling parameters for the simulations: number of basis vectors per configuration K, number of configurations N, compression for the two bath modes α^{b}, execution time t for one propagation step on 1 and 16 processors, where one CCS step is taken as unity.

Method	K	N	$K \times N$	α^{b}	$t_{CCS=1}$ 1 proc	$t_{CCS=1}$ 16 proc
CCS	1	2000	2000	0.8	1.0	1.0
2L-CCS	1	2000	2000	0.8	1.0	1.0
2L-CCS	2	2000	4000	0.8	3.8	2.4
2L-CCS	4	2000	8000	0.8	14.5	7.8
2L-CCS	4	100	400	5.0	0.04	0.02
2L-CCS	4	500	2000	1.2	0.9	0.5

Increasing the number of configurations N also allows the value of α^{b} to be reduced whilst maintaining a norm close to unity. This effect has been previously demonstrated in Ref. 16 and can be applied in the same manner for both CCS and 2L-CCS. For example, when $N = 2000$, a value of $\alpha^{\mathrm{b}} = 0.8$ was used for both CCS and 2L-CCS, whilst for $N = 100$, a value of $\alpha^{\mathrm{b}} = 5.0$ was used. Table I compares the initial bath samplings used for various K and N parameters. The tunnelling mode is sampled from a relatively broad distribution around the initial wavepacket coordinates $q^{(1)}(0) = -2.5$ and $p^{(1)}(0) = 0.0$, as in previous work,[36] with compression parameter $\alpha^{\mathrm{s}} = 1.0$ for all values of K and N.

Calculation of the initial amplitudes proceeds in two stages: first, the set of K amplitudes for a given configuration n is obtained via projection of the initial "quantum" coherent state distribution $|\mathbf{z}_{kn}^{(\mathrm{q})}\rangle$ onto the initial wavepacket for the tunnelling mode $|\Psi^{(\mathrm{q})}(0)\rangle$,

$$\langle\mathbf{z}_{ln}^{(\mathrm{q})}|\Psi^{(\mathrm{q})}(0)\rangle = \sum_{k=1}^{K} d_{kn}(0)\langle\mathbf{z}_{ln}^{(\mathrm{q})}|\mathbf{z}_{kn}^{(\mathrm{q})}\rangle. \quad (28)$$

Once the initial d_{kn} amplitudes have been calculated for all N configurations, the $D_n(0)$ amplitudes may be determined by projection of the entire initial coherent state distribution $|\mathbf{z}_{kn}\rangle$ onto the entire initial wavepacket $|\Psi(0)\rangle$,

$$\langle\mathbf{z}_{lm}(0)|\Psi(0)\rangle = \sum_{n=1}^{N} D_n(0) \sum_{k=1}^{K} d_{kn}(0)\langle\mathbf{z}_{lm}(0)|\mathbf{z}_{kn}(0)\rangle. \quad (29)$$

D. Comparison of the 2L-CCS method with standard CCS and against benchmark results

In this section, 2L-CCS is compared with standard CCS and against the benchmark calculations for coupling parameter $\lambda = 0.1$, for which results from MP/SOFT[35] and CI expansion[37] methods are also available. The CCS results are re-calculated in this work, rather than using those from Ref. 36 in view of the improved sampling procedure mentioned in Sec. III C. In the CCS calculations, all modes are governed by CCS equations (13) and (15)–(17) with the complete system wavefunction having the form of Eq. (1). In the 2L-CCS calculations, CCS equations (13) and (15)–(17) are used for the tunnelling mode only, while the time-evolution of the bath

modes is determined by Ehrenfest trajectories (18), which give rise to Eq. (24). Standard CCS with the basis of N CSs can be regarded as 2L-CCS with N configurations and with a single ($K = 1$) CS in each configuration.

The quantity of interest is the cross-correlation function (CCF) between the wavefunction at time t and mirror image of the initial state $|\bar{\Psi}(0)\rangle$, i.e., the overlap $\langle\bar{\Psi}(0)|\Psi(t)\rangle$. The mirror state coordinates are $\bar{q}^{(1)}(0) = +2.5$ and $\bar{p}^{(1)}(0) = 0.0$ with all bath mode coordinates and momenta set to zero. Since the mirror state is located in an upper local energy minimum, non-zero values of the CCF are indicative of tunnelling. The power spectra calculated by taking the Fourier transform of the CCF as

$$I(\omega) = \int_0^T \mathrm{Re}[\langle\bar{\Psi}(0)|\Psi(t)\rangle]e^{-i\omega t}dt \tag{30}$$

will also be used for comparisons among the different methods and is used as an indication of the long-term propagation accuracy. The total propagation time $T = 120$ time units for all methods. The comparison of the results from various methods[35,37,38] can be seen in Fig. 1 for the cross-correlation function and in Fig. 2 for the Fourier transforms. Both CCS and 2L-CCS cross-correlation functions compare well to the other methods and the benchmark at early time scales ($t < 25$ a.u.), and the Fourier spectra have peaks of the same frequencies and similar intensities. However, the splitting of the peaks in the spectra is not well reproduced by CCS and 2L-CCS, which may be explained by two reasons. First, the basis does not effectively cover the high energy region; hence, the high frequency peaks are not faithfully reproduced. A similar effect was found with CCS when applied to the far infrared absorption spectrum of a water trimer in Ref. 39. Second, the splitting of the lower energy peak at $\omega = 9.5$ is not as large for CCS and 2L-CCS as it is for the benchmark because it does not begin to appear until 50 a.u. into the benchmark calculation, and by this point, Monte Carlo noise has begun to affect the CCS and 2L-CCS calculations, reducing their accuracy.

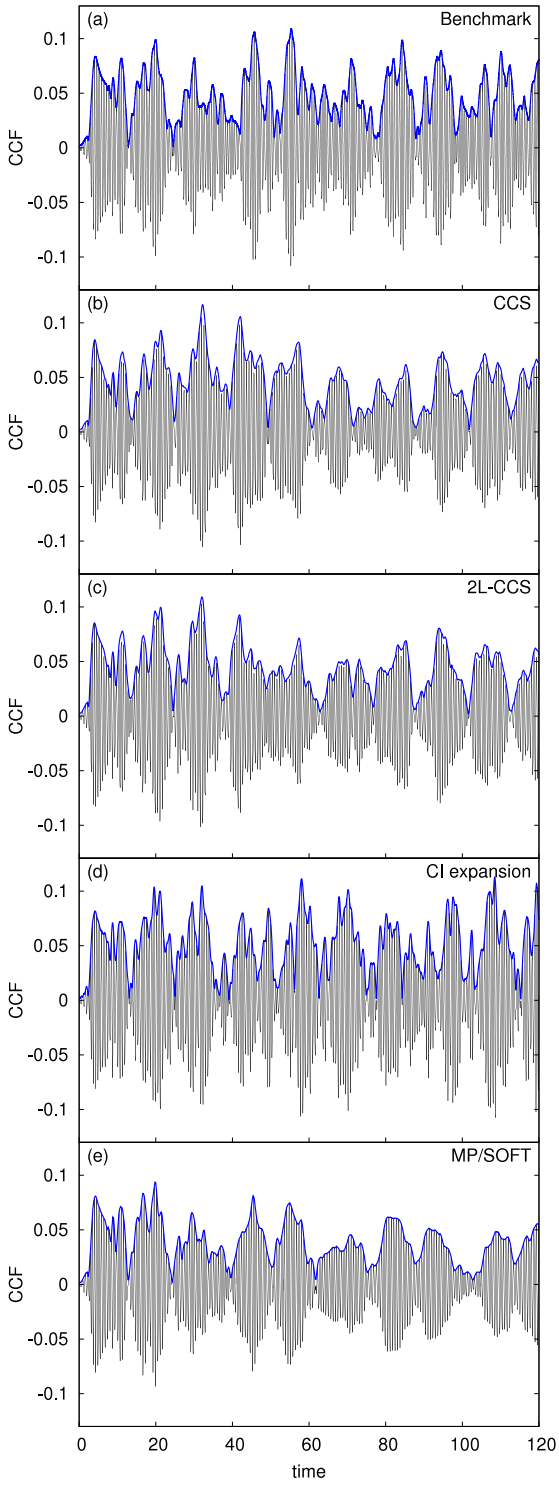

FIG. 1. Comparison of cross-correlation functions: (a) benchmark, (b) CCS (2000 confs), (c) 2L-CCS (4 CSs/2000 confs), (d) CI expansion, and (e) MP/SOFT.

The CCS and 2L-CCS calculations can both be converged by increasing the number of configurations N, whilst 2L-CCS has the additional flexibility of increasing the number of basis vectors K per configuration for convergence. As 2L-CCS uses a random sampling of basis functions, like CCS, it will be plagued by noise inherent to the method and propagation will be most accurate for short time scales, as mentioned above. Therefore, for these short time scales, we should expect the calculation to converge towards the benchmark result, which is what is shown in Figs. 3 and 4. It can be seen in Fig. 3 that the quality of short-term propagation is affected by the number of basis vectors per configuration: the larger the value of K for the same number of configurations, the better the result. This is illustrated qualitatively in panels (a)–(c) by the amplitude and phase of the 2L-CCS CCF more closely matching that of the benchmark for increasing K. In panel (d), χ is defined at the integral over $|\ \mathrm{Abs}(\langle\bar{\Psi}(0)|\Psi(t)\rangle)_{\mathrm{bench}} - \mathrm{Abs}(\langle\bar{\Psi}(0)|\Psi(t)\rangle)_{\text{2L-CCS}}\ |$ in the time period shown, a measure of the cumulative error of the 2L-CCS method. This quantitatively demonstrates 2L-CCS converging with respect to K, as χ decreases with increasing K.

The quality of short-term propagation also improves with increasing number of configurations, whilst keeping K fixed, as can be seen in Fig. 4. This is illustrated qualitatively in panels (a)-(c) once more, with the amplitude and phase of the 2LCCS CCF more closely matching that of the benchmark for increasing N, and shown quantitatively in panel (d) with decreasing χ for increasing N.

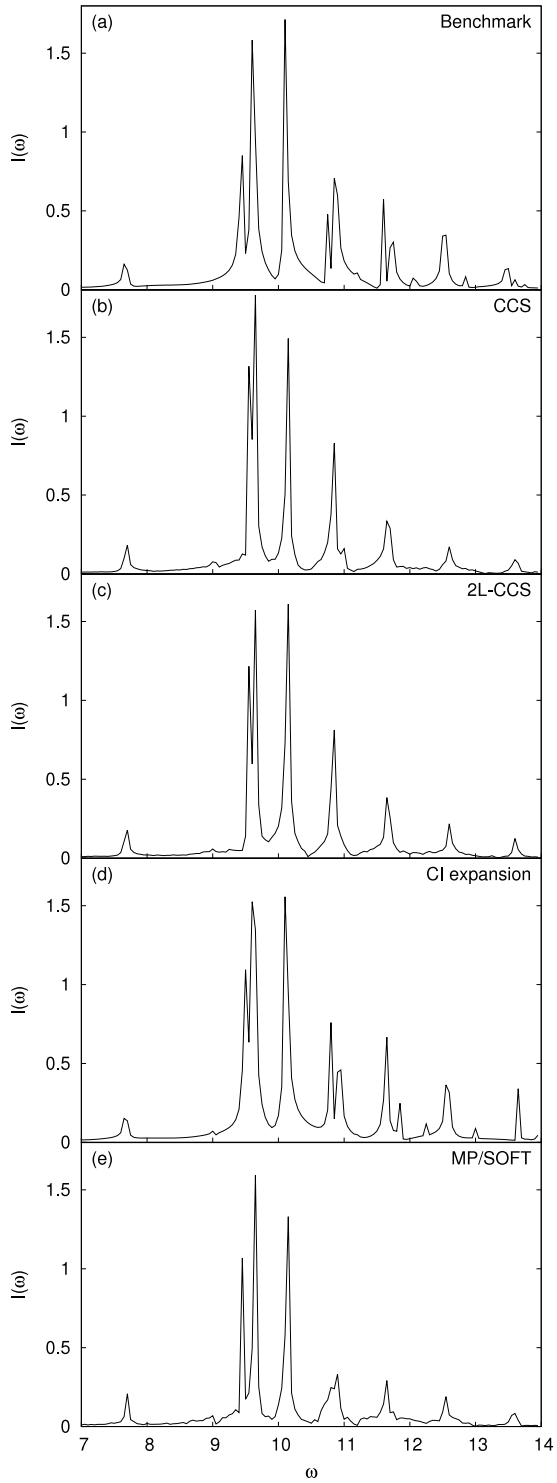

FIG. 2. Comparison of Fourier transforms: (a) benchmark, (b) CCS (2000 confs), (c) 2L-CCS (4 CSs/2000 confs), (d) CI expansion, and (e) MP/SOFT.

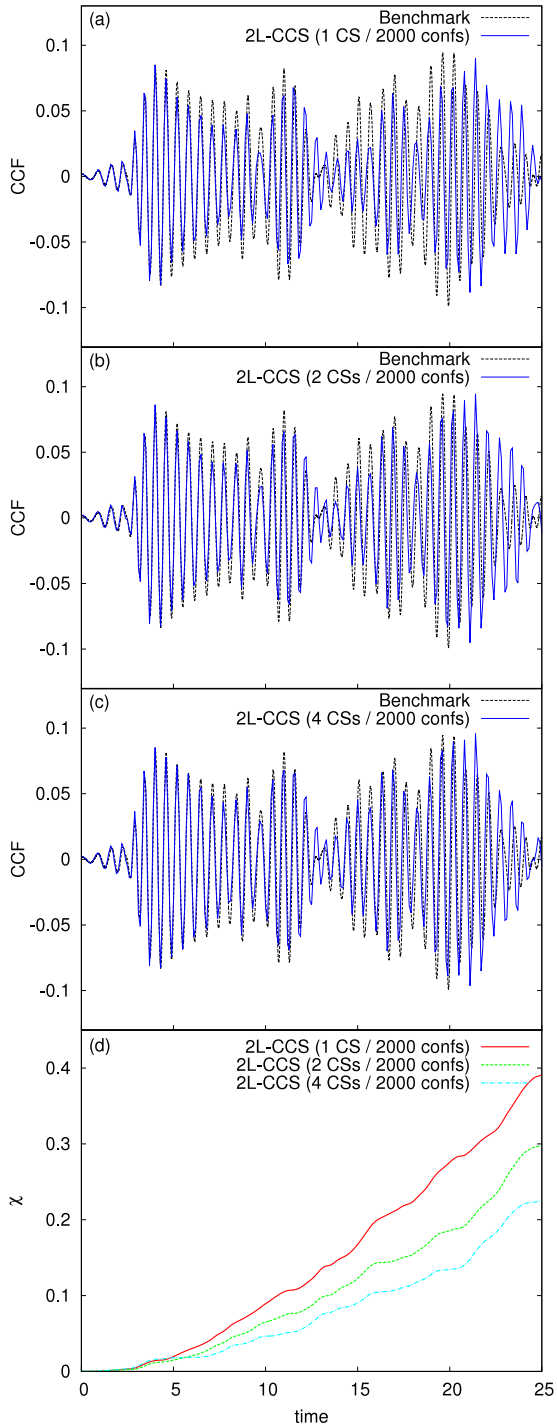

FIG. 3. Comparison of short-term CCF from benchmark and 2L-CCS: (a) 1 CS/2000 confs, (b) 2 CSs/2000 confs, and (c) 4 CSs/2000 confs. (d) shows the cumulative error χ, defined in the text, between the benchmark and 2L-CCS calculations.

Whilst 2L-CCS will be most accurate for short time scales, it is of course worthwhile to check the long time propagation accuracy of the method, accessed via the Fourier-transform of the cross-correlation function after $t = 120$ a.u. This is shown in Figs. 5 and 6. In this longer time scale we might expect that the calculation will improve relative to the benchmark as we increase K and N, up until a point where the effect of Monte Carlo noise at later times outweighs the improvements made at earlier times and no further change in the spectra is observed. It can be seen from Fig. 5 that the Fourier-transform is getting closer to the benchmark as K increases for the same value of N, although the difference is not very significant. Increasing the number of configurations has a more profound effect on the long-term accuracy, shown in Fig. 6, which indicates that for this particular problem, improving the treatment of the bath via increasing N is more important for long-term accuracy than improving treatment of

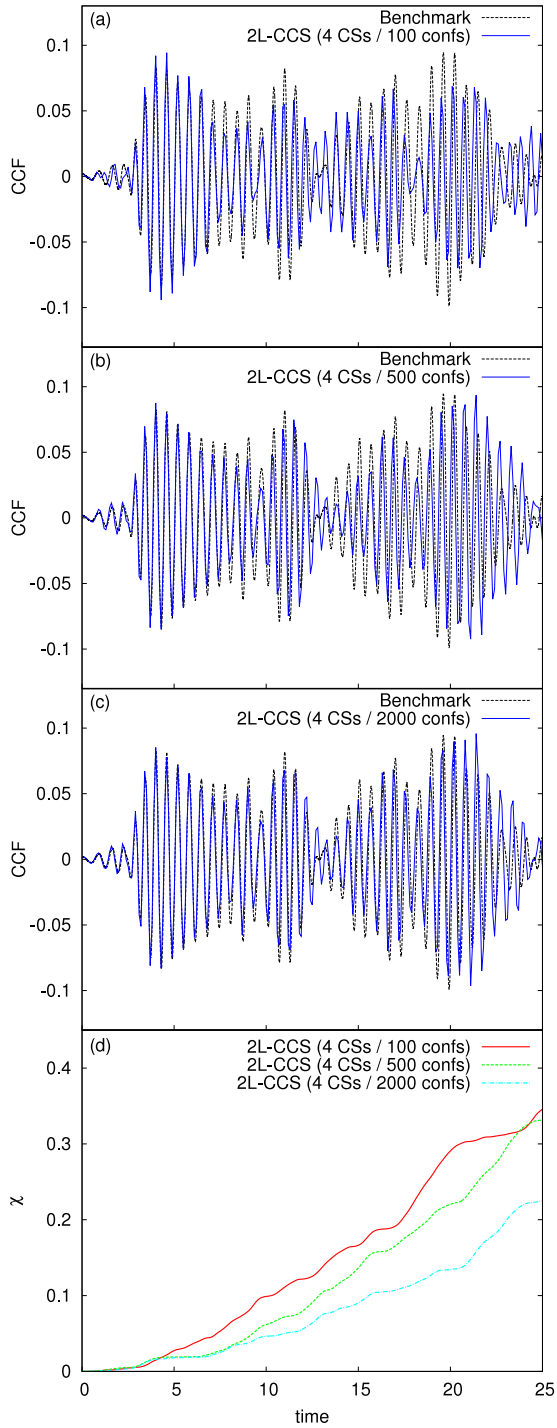

FIG. 4. Comparison of short-term CCF from benchmark and 2L-CCS: (a) 4 CSs/100 confs, (b) 4 CSs/500 confs, and (c) 4 CSs/2000 confs. Panel (d) shows the cumulative error χ, defined in the text, between the benchmark and 2L-CCS calculations.

the system via increasing K. In Table I, it can be seen that by raising the number of configurations, the bath compression α^{b} can be reduced until a stable propagation with good norm-conservation can be obtained. By decompressing the bath modes, a greater dynamical region can be covered by the coherent states, precisely the effect that was discussed in Sec. III C.

Despite the fact that increasing N improved the long-term accuracy of this calculation more than increasing K, the fact

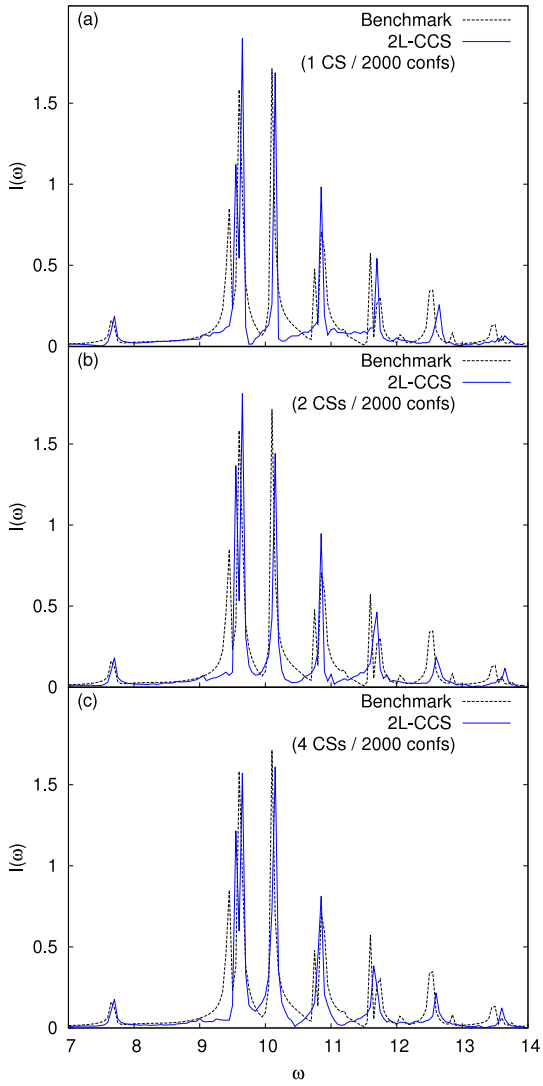

FIG. 5. Comparison of Fourier-transforms from benchmark and 2L-CCS: (a) 1 CS/2000 confs, (b) 2 CSs/2000 confs, and (c) 4 CSs/2000 confs.

that increasing both improved the quality of the calculation to some degree demonstrates the additional layer of flexibility that 2L-CCS presents. This property may be extremely useful for tackling other composite problems, especially those where the tunnelling mode may be more complex to represent.

E. Comparison of numerical performance of the 2L-CCS and the standard CCS methods

The time step of integration for both standard CCS and 2L-CCS was $\Delta t = 0.1$ a.u., which gave good norm-conservation for both cases. Numerically, the two-layer method scales with the number of basis vectors K and the number of configurations N, but its performance—similarly to CCS—does not depend explicitly on the number of degrees of freedom. This is due to the fact that neither CCS Eqs. (13) and (15)–(17) nor Ehrenfest-equation (18) scales directly with the dimensionality.

For the standard CCS method with N configurations, $N \times N$ linear system has to be solved at each time step. For 2L-CCS with K basis vectors per configuration, (16) has to be solved N times (once per configuration) every time step, but

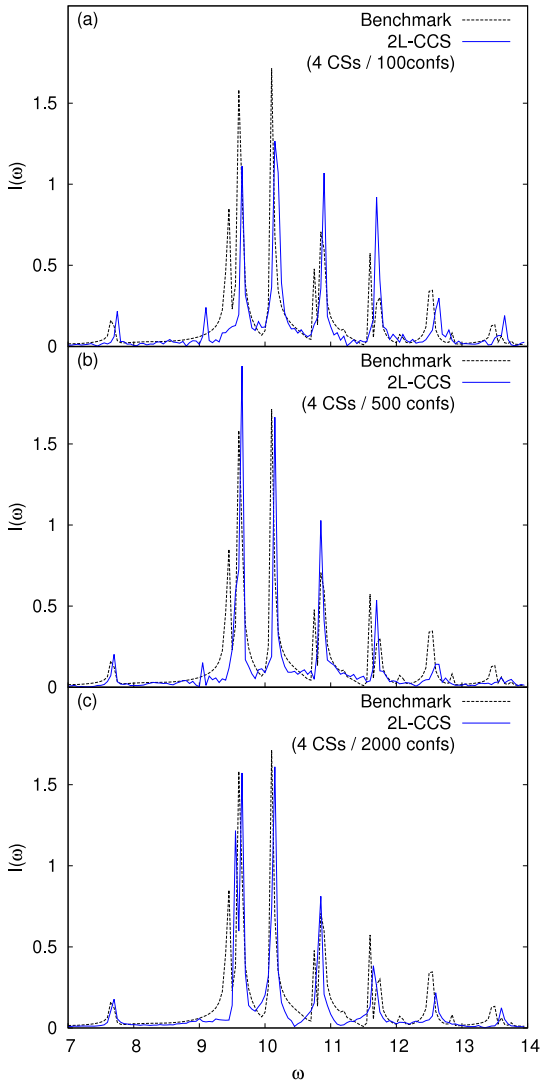

FIG. 6. Comparison of Fourier-transforms from benchmark and 2L-CCS: (a) 4 CSs/100 confs, (b) 4 CSs/500 confs, and (c) 4 CSs/2000 confs.

the size of each linear system is $K \times K$. In addition, (19) has to be solved for amplitude D, which involves a linear system of size $N \times N$. Solving N linear systems of size $K \times K$ and one linear system of size $N \times N$ is more efficient than solving a single $[K \times N] \times [K \times N]$ linear system, as long as K and N are adequately balanced. This means that 2L-CCS will be numerically favourable to a CCS calculation that has $K \times N$ configurations. The comparison of the numerical performance of the two methods can be seen in Table I. The CCS calculation with 2000 configurations and the 2L-CCS calculation with 500 configurations and 4 basis vectors per configuration illustrate the point made above. Although this 2L-CCS calculation is only twice as fast as the CCS calculation on 16 processors, for problems where K and N can be more evenly balanced (such as real problems with more complicated tunnelling effects), this effect will be significantly enhanced.

The 2L-CCS calculation also benefits from parallelisation to a greater extent than CCS, partially demonstrated in Table I and more profoundly shown in Fig. 7. For both CCS and 2L-CCS, as the number of processors increases the bottleneck of the calculation comes from solution of the system of N

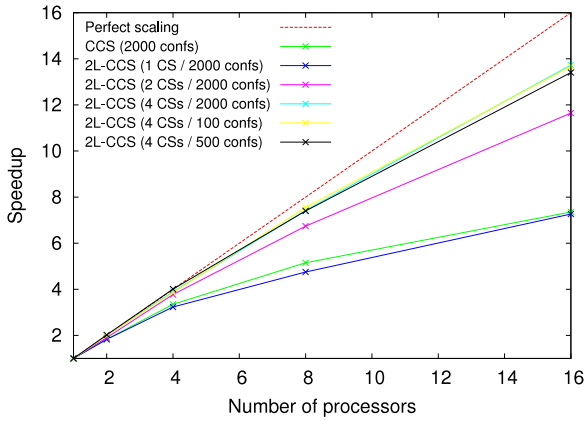

FIG. 7. Parallel speedup for the CCS and 2L-CCS calculations studied in this paper.

linear equations. However, in 2L-CCS, a propagation step also involves the solution of N lots of a system of K linear equations, Eq. (16), which is much quicker. Therefore, the rest of the 2L-CCS propagation step can be sped up around the solution of the system of N linear equations, leading to greater parallel efficiency. It should be noted that this speedup does not take into account basis set generation, as the parallel speedup is based on a propagation step only; however, basis set generation is rapid in comparison to propagation. Also, in Fig. 7, the speedup of 2L-CCS (1 CS/2000 confs) is slightly below that of CCS (2000 confs), despite being equivalent calculations. The reason for this is that in 2L-CCS, the time dependence of two amplitudes is calculated every propagation step (16) and (19), whereas in CCS, only one is calculated.

The OpenMP shared memory construct was used to parallelise both CCS and 2L-CCS, requiring very little modification of the serial code. This did limit the number of threads to a maximum of 16, as computational hardware with 16 processors was used for the calculations and the general rule of thumb of 1 processor per thread was obeyed. For larger and more complicated calculations, Message Passing Interface (MPI) parallelisation can be used, although this may require significant restructuring of the serial code. We leave this to further investigation.

IV. CONCLUSIONS

In this paper, a two-layer scheme has been proposed for Gaussian based quantum dynamics, motivated by the MCE[19,20] and CCS[8,14–16] methods. Multilayer schemes are known in other approaches to quantum dynamics, such as the ML-MCTDH[3–5] and ML-G-MCTDH[6] methods, and the current paper introduces similar ideas for a Gaussian based trajectory guided technique. The scheme allows a flexible representation of the wavefunction and enables the use of different dynamical descriptions for different subsystems of the whole quantum mechanical system. The inner "quantum" system is represented by CCS dynamics, whilst the outer "classical" bath uses Ehrenfest trajectories. The 2L-CCS method may therefore be seen as a version of MCE where Gaussian CSs are used as a basis for both "quantum" subsystem and "classical" bath.

The scheme was tested on a 20-dimensional asymmetric double well potential previously studied by the CCS,[36] MP/SOFT,[35] and CI expansion[37] methods. The 2L-CCS method was found to compare favourably with previous results and with a benchmark study on the potential.[38] The scheme was found to converge in both the short and long time scales by increasing the number of "quantum" basis vectors per configuration, K, and the number of configurations, N. Both the short and long term propagation represented an improvement over standard CCS, although admittedly it was not significantly closer to the benchmark. However, the purpose of the test with Hamiltonian (22) was to show that the 2L-CCS method works and converges appropriately. The aim of the scheme is to be implemented in the form of on-the-fly direct dynamics for which the improved treatment of tunnelling that 2L-CCS offers over CCS will be extremely beneficial for more challenging real problems.

The 2L-CCS method can also represent an increase in numerical efficiency over the CCS method. For example, a given 2L-CCS calculation which uses K basis vectors and N configurations will be more numerically efficient than an equivalent CCS calculation which uses $K \times N$ configurations. For calculations where K and N can be adequately balanced, this effect will be significant. Furthermore, 2L-CCS can benefit greatly from parallelisation, leading to a greater speedup for a propagation step than CCS on the same number of processors.

The application of 2L-CCS to Hamiltonian (22) provided a valid test of an interesting new propagation scheme and illustrated the flexibility of the wavefunction representation. This can lead to further investigation on composite systems where the quantum and the classical modes can be separated. Furthermore, since the method is particularly accurate for short-time scales, it may be combined with a basis set reprojection technique, allowing accurate propagation for a short time period until the basis is required to be re-centered and propagated again for another short time period. Both these advantages of the 2L-CCS method may be utilised for problems such as the modelling of high-order harmonic generation[40] where the "principal" mode, the motion of an electron which is aligned in the direction of the field, is "quantum" and the other degrees of freedom are "classical." Investigation is underway.

ACKNOWLEDGMENTS

This work was supported by the EPSRC Grant Nos. EP/J019240/1 and EP/I014500/1. A.G. would like to acknowledge financial support from FAPESP under Grant No. 2013/00145-9. J.A.G. is supported by the University Research Scholarship from the University of Leeds. D.V.S. and M.R. gratefully acknowledge V. Batista and S. Habershon for providing their data.

APPENDIX A: DERIVING THE WORKING EQUATIONS

In this appendix, the equations for the 2L-CCS method are derived. As mentioned in Sec. II, they do not follow from a full variational treatment of the complete wavefunction—where all parameters are optimised at once—but rather from a hierarchical optimisation procedure, where the TDVP[41] is applied to different subsets of parameters at a time. The dynamics of the first layer quantum modes $\mathbf{z}_{kn}^{(\mathrm{q})}$ is prescribed according to equations of motion that follow from the TDVP applied to a single CS. In turn, the dynamics of coefficients a_{kn} and classical coordinates $\mathbf{z}_n^{(\mathrm{c})}$ follows from the TDVP applied to individual configurations $|\phi_n\rangle$ (and with the $\mathbf{z}_{kn}^{(\mathrm{q})}$ regarded as simple time-dependent functions). The second layer amplitudes D_n have their dynamics determined from the TDVP applied to the complete wavefunction (with the configurations $|\phi_n\rangle$ regarded as a guided basis set).

Let us briefly recall the basic concepts of the TDVP: suppose we are given a trial state $|\psi\rangle$, not necessarily normalised, parametrised by a set of n real parameters $(\xi_1, \xi_2, \ldots, \xi_n)$;[42] this is abbreviated as $\psi = \psi(\xi)$. The equations of motion for the time-dependent parameters ξ are obtained by making the action functional $S[\psi] = \int_{t_1}^{t_2} \mathcal{L} dt$ stationary under the boundary conditions: $\delta\psi(t_1) = \delta\psi^*(t_1) = 0$ and $\delta\psi(t_2) = \delta\psi^*(t_2) = 0$; here, the Lagrangian $\mathcal{L}$ is

$$\mathcal{L}(\xi, \dot{\xi}) = \frac{i}{2} \frac{\langle\psi|\dot{\psi}\rangle - \langle\dot{\psi}|\psi\rangle}{\langle\psi|\psi\rangle} - \frac{\langle\psi|\hat{H}|\psi\rangle}{\langle\psi|\psi\rangle}. \tag{A1}$$

The stationary condition $\delta S = 0$ leads directly to the Euler-Lagrange equations,

$$\frac{\partial \mathcal{L}}{\partial \xi_l} - \frac{d}{dt}\frac{\partial \mathcal{L}}{\partial \dot{\xi}_l} = 0 \quad \text{for} \quad l = 1, \ldots, n \tag{A2}$$

provided all variations $\delta\xi_l$ can be performed independently. From (A2), the equation of motion for each of the ξ_l follows.

The variational solution $\psi(t) = \psi(\xi(t))$ obtained in this way represents the best achievable solution with the limited set of parameters ξ. If there is a sufficient number of parameters (i.e., if the trial state proves to be flexible enough), this solution will converge to the exact solution of the Schrödinger equation for the particular system at hand, as long as normalisation is ensured and a proper phase factor, which is just the action $S(\psi(t)) = S(\xi(t))$ evaluated over the orbit $\xi(t)$, is added to $|\psi\rangle$.[43] The resulting wavefunction $|\Psi(t)\rangle$ relates to $|\psi(t)\rangle$ in the following way:

$$|\Psi(t)\rangle = \frac{|\psi(t)\rangle}{\sqrt{\langle\psi(t)|\psi(t)\rangle}} e^{iS(\psi(t))}. \tag{A3}$$

The overall action phase is immaterial if $|\Psi(t)\rangle$ is to be regarded as the complete wavefunction of the system in question. However, the fundamental strategy of the present method is to express the system's complete wavefunction as a linear combination of such variationally optimised solutions, which then act as a guided basis. In this scenario, the phase plays an important role in smoothing out oscillations thus allowing for a more accurate description of interference effects between the basis elements.

1. Single CS dynamics

The fundamental block in the standard CCS method and all its variants is the single coherent state: $|\psi\rangle = |\mathbf{z}\rangle$. When $|\mathbf{z}\rangle$ is used as a trial state in Eq. (A1), we obtain the Lagrangian,

$$\mathcal{L} = \frac{i}{2}(\mathbf{z}^*\dot{\mathbf{z}} - \dot{\mathbf{z}}^*\mathbf{z}) - H_{ord}(\mathbf{z}^*, \mathbf{z}), \tag{A4}$$

where the ordered Hamiltonian H_{ord} is like in Eq. (12). Taking $\mathbf{z}$ and $\mathbf{z}^*$ as independent variables, Euler-Lagrange equations (A2) translate to

$$\frac{\partial \mathcal{L}}{\partial \mathbf{z}^*} - \frac{d}{dt}\frac{\partial \mathcal{L}}{\partial \dot{\mathbf{z}}^*} = 0 \tag{A5}$$

plus an equivalent complex conjugate equation. The equation of motion for $\mathbf{z}$ follows immediately

$$\dot{\mathbf{z}} = -i\frac{\partial H_{ord}(\mathbf{z}^*,\mathbf{z})}{\partial \mathbf{z}^*} \tag{A6}$$

which is just the familiar pair of Hamilton equations from classical mechanics, but written in complex notation. The optimised state in this case would be $|\mathbf{z}(t)\rangle e^{iS(\mathbf{z}(t))}$.

2. First layer ("quantum" modes)

The prototype system suitable for the method is an M-dimensional system composed of two sub-systems: the first contains a total of $M^{(\mathrm{q})}$ "quantum" DOF and the second corresponds to the remaining "classical" DOF. The configurations $|\varphi_n\rangle$ in Eq. (8) read[44]

$$|\varphi_n\rangle = \left[\sum_{k=1}^{K} b_{kn}|\mathbf{z}_{kn}^{(\mathrm{q})}\rangle\right]|\mathbf{z}_m^{(\mathrm{c})}\rangle \tag{A7a}$$

$$= \sum_{k=1}^{K} b_{kn}|\mathbf{z}_{kn}\rangle, \tag{A7b}$$

where in the second line, the primitive CS basis is abbreviated as $|\mathbf{z}_{kn}\rangle = |\mathbf{z}_{kn}^{(\mathrm{q})}\rangle|\mathbf{z}_m^{(\mathrm{c})}\rangle$. The parameters of each $|\varphi_n\rangle$ have to be optimised individually, so that later, these configurations can be used as a guided basis when expressing the complete wavefunction.

However, when taking (A7) as a trial-state, we shall regard as variational parameters only the set of coefficients b_{kn} and the "classical" coordinates $\mathbf{z}_n^{(\mathrm{c})}$. The "quantum" coordinates $\mathbf{z}_{kn}^{(\mathrm{q})}$, meanwhile, will have their dynamics *prescribed* according to the single CS result, Eq. (A6) [which in the present context translates to Eq. (13) of Sec. II]. This is done in order to avoid complicated equations of motion for the coordinates $\mathbf{z}_{kn}^{(\mathrm{q})}$ which would otherwise result from the variational procedure.

The first step would be to write down the Lagrangian $\mathcal{L}$ of Eq. (A1) taking $|\psi\rangle = |\varphi_n\rangle$. However, owing to the non-orthogonality of the CSs used in Eq. (A7), this straightforward approach leads to somewhat cumbersome Euler-Lagrange equations.

Aiming at a simpler derivation, we proceed as follows: using a sub-index n to refer to quantities calculated within the n-th configuration, and denoting the norm by

$$N_n = \langle\varphi_n|\varphi_n\rangle = \sum_{kl=1}^{K} b_{kn}^*\langle\mathbf{z}_{kn}^{(\mathrm{q})}|\mathbf{z}_{ln}^{(\mathrm{q})}\rangle b_{ln}, \tag{A8}$$

the Lagrangian

$$\mathcal{L}_n = \frac{i}{2}\frac{\langle\varphi_n|\dot{\varphi}_n\rangle - \langle\dot{\varphi}_n|\varphi_n\rangle}{\langle\varphi_n|\varphi_n\rangle} - \frac{\langle\varphi_n|\hat{H}|\varphi_n\rangle}{\langle\varphi_n|\varphi_n\rangle} \tag{A9}$$

may be expressed as

$$\mathcal{L}_n = \frac{L_n}{N_n} - \frac{i}{2}\frac{d\log N_n}{dt}, \tag{A10}$$

where the implicitly defined L_n, given by

$$L_n = i\langle\varphi_n|\dot{\varphi}_n\rangle - \langle\varphi_n|\hat{H}|\varphi_n\rangle \tag{A11}$$

is exactly $\mathcal{L}_n(N_n = 1)$.

We wish to work with L_n rather than with $\mathcal{L}_n$, but we cannot simply make $N_n = 1$ in the action functional, as this prevents us from performing independent variations of the amplitudes b_{kn}, which is a necessary assumption if the Euler-Lagrange equations are to be obtained. To overcome this, a Lagrange multiplier λ_n is introduced in the action functional to take care of the constrain $N_n = 1$; thus, the action can be rewritten as

$$S_n = S[\lambda_n,\varphi_n] = \int_{t_1}^{t_2}\left(\frac{L_n}{N_n} - \lambda_n(N_n - 1)\right)dt, \tag{A12}$$

where the surface terms that come from the derivative $-\frac{i}{2}\frac{d\log N_n}{dt}$ of Eq. (A10) have been omitted for which they vanish trivially upon variation of S_n.

Let us temporarily denote by $\{\alpha_l^*,\alpha\}$ the set of (complex) parameters of the trial state: $|\varphi_n\rangle = |\varphi_n(\alpha^*,\alpha)\rangle$. If we impose the condition $\delta S_n = 0$ and use the fact that variations $\{\delta\lambda,\delta\alpha_l^*,\delta\alpha_l\}$ are now all independent, we find that the following set of equations must hold:

$$\frac{1}{N_n}\left(\frac{\partial L_n}{\partial \alpha_l^*} - \frac{d}{dt}\frac{\partial L_n}{\partial \dot{\alpha}_l^*}\right) - \left(\lambda_n + \frac{L_n}{N_n^2}\right)\frac{\partial N_n}{\partial \alpha_l^*} = 0, \tag{A13a}$$

$$\frac{1}{N_n}\left(\frac{\partial L_n}{\partial \alpha_l} - \frac{d}{dt}\frac{\partial L_n}{\partial \dot{\alpha}_l}\right) - \left(\lambda_n + \frac{L_n}{N_n^2}\right)\frac{\partial N_n}{\partial \alpha_l} = 0, \tag{A13b}$$

$$N_n - 1 = 0. \tag{A13c}$$

We shall work with this alternative form of the Euler-Lagrange equations rather than the one in Eq. (A2).

Substituting the configuration ansatz of Eq. (A7), into the Lagrangian L_n of Eq. (A11), it reads

$$L_n = i\sum_{kl=1}^{K}\left(b_{kn}^*\langle\mathbf{z}_{kn}^{(\mathrm{q})}|\mathbf{z}_{ln}^{(\mathrm{q})}\rangle\dot{b}_{ln} + b_{kn}^*\langle\mathbf{z}_{kn}^{(\mathrm{q})}|\dot{\mathbf{z}}_{ln}^{(\mathrm{q})}\rangle b_{ln}\right)$$
$$+ \frac{i}{2}(\mathbf{z}_n^{(c)*}\dot{\mathbf{z}}_n^{(\mathrm{c})} - \dot{\mathbf{z}}_n^{(c)*}\mathbf{z}_n^{(\mathrm{c})}) - \langle\phi_n|\hat{H}|\phi_n\rangle. \tag{A14}$$

Following this, the set of Equations (A13) can be rewritten in terms of the different parameters of the trial state: for the classical mode coordinates, we get immediately from Eq. (A13a) the following:

$$\frac{\partial L_n}{\partial \mathbf{z}_n^{(c)*}} - \frac{d}{dt}\frac{\partial L_n}{\partial \dot{\mathbf{z}}_n^{(c)*}} = 0 \tag{A15}$$

since N_n does not depend upon these coordinates. This leads at once to the Ehrenfest equation

$$\dot{\mathbf{z}}_n^{(\mathrm{c})} = -i\sum_{kl=1}^{K} b_{kn}^* b_{kl}\langle\mathbf{z}_{kn}^{(\mathrm{q})}|\mathbf{z}_{ln}^{(\mathrm{q})}\rangle\frac{\partial H_{ord}(\mathbf{z}_{kn}^*,\mathbf{z}_{kl})}{\partial \mathbf{z}_n^{(c)*}}, \tag{A16}$$

which shows that the "classical" modes $\mathbf{z}_n^{(\mathrm{c})}$ experience a potential averaged over all sets of quantum modes.

On the other hand, for the amplitudes b_{kn}, Eqs. (A13) reduce to

$$\frac{\partial L_n}{\partial b_{kn}} - \frac{d}{dt}\frac{\partial L_n}{\partial \dot{b}_{kn}} - (\lambda_n + L_n)\frac{\partial N_n}{\partial b_{kn}} = 0, \quad \text{(A17a)}$$

$$\frac{\partial L_n}{\partial b^*_{kn}} - (\lambda_n + L_n)\frac{\partial N_n}{\partial b^*_{kn}} = 0. \quad \text{(A17b)}$$

These two equations are equivalent but, since $\dot{b}^*_{kn}$ does not appear in L_n, it is easier to work with the second one. Moreover, because N_n is linear in the amplitudes, we can easily find λ_n by multiplying Eq. (A17b) with b^*_{kn}, summing over k and using the fact that $N_n = 1$; this gives

$$\lambda_n + L_n = \sum_{k=1}^{K} b^*_{kn}\frac{\partial L_n}{\partial b^*_{kn}}, \equiv \dot{\upsilon}_n, \quad \text{(A18)}$$

where the quantity $\dot{\upsilon}_n$ is defined for convenience. Hence, combining Eqs. (A18) and (A17b), it follows that

$$\sum_{l=1}^{K}\langle \mathbf{z}^{(\mathrm{q})}_{kn}|\mathbf{z}^{(\mathrm{q})}_{ln}\rangle(i\dot{b}_{ln} - \dot{\upsilon}_n b_{ln}) = \sum_{l=1}^{K}\langle \mathbf{z}^{(\mathrm{q})}_{kn}|\mathbf{z}^{(\mathrm{q})}_{ln}\rangle\left[H(\mathbf{z}^*_{kn}, \mathbf{z}_{ln}) - i\frac{\langle \mathbf{z}^{(\mathrm{q})}_{kn}|\dot{\mathbf{z}}^{(\mathrm{q})}_{ln}\rangle}{\langle \mathbf{z}^{(\mathrm{q})}_{kn}|\mathbf{z}^{(\mathrm{q})}_{ln}\rangle}\right] b_{ln}. \quad \text{(A19)}$$

Finally, we introduce new amplitudes d_{nk} according to the following transformation:

$$b_{kn} = (d_{kn}e^{iS^{(\mathrm{q})}_{kn}})e^{-i\upsilon_n} = (a_{kn}e^{-i\theta^{(\mathrm{c})}_n})e^{-i\upsilon_n}, \quad \text{(A20)}$$

where a_{kn} are identified as the coefficients in (8) and $S^{(\mathrm{q})}_{kn}$ is the quantity

$$S^{(\mathrm{q})}_{kn} = \int_0^t \left[\frac{i}{2}(\mathbf{z}^{(q)*}_{kn}\dot{\mathbf{z}}^{(\mathrm{q})}_{kn} - \dot{\mathbf{z}}^{(q)*}_{kn}\mathbf{z}^{(\mathrm{q})}_{kn}) - H_{ord}(\mathbf{z}^*_{kn}, \mathbf{z}_{kn})\right] dt' \quad \text{(A21)}$$

which can be interpreted as the action of the quantum modes with the classical subsystem regarded as an external system.

The purpose of the change of variables in Eq. (A20) is threefold: first, it effectively cancels the $\dot{\upsilon}_n$ on the left-hand side of Eq. (A19); second, the derivative of the action $\dot{S}^{(\mathrm{q})}_{ln}$, when combined with the remaining terms on the right-hand side of Eq. (A19), gives the familiar CCS equation for the new amplitudes d_{kn}—which is exactly Eqs. (16) and (17) of Sec. II—and third, if the configuration $|\varphi_n\rangle$ is rewritten together with its phase $S(\varphi_n)$ [as it appears in the full wavefunction ansatz; see Eq. (A23)] in terms of the new amplitudes d_{kn}, we recover the optimised phase for the quantum basis functions,

$$|\varphi_n\rangle e^{iS(\varphi_n)} = \left[\sum_{k=1}^{K} d_{kn}|\mathbf{z}^{(\mathrm{q})}_{kn}\rangle e^{iS^{(\mathrm{q})}_{kn}}\right]|\mathbf{z}^{(\mathrm{c})}_n\rangle e^{i\theta^{(\mathrm{c})}_m} \quad \text{(A22a)}$$

$$= \sum_{k=1}^{K} d_{kn}|\mathbf{z}_{kn}\rangle e^{iS_{kn}}, \quad \text{(A22b)}$$

where in the last equation S_{kn} is the action defined in Eq. (15) of Sec. II. Notice that when we write the configuration as in (A22a), explicitly separating the subsystems, we see that the "classical" modes $|\mathbf{z}^{(\mathrm{c})}_n\rangle$ are left with a geometric phase $\theta^{(\mathrm{c})}_n = \frac{i}{2}\int_0^t(\mathbf{z}^{(c)*}_n\dot{\mathbf{z}}^{(c)}_n - \dot{\mathbf{z}}^{(c)*}_n\mathbf{z}^{(\mathrm{c})}_n)dt'$.

3. Second layer ("classical" modes)

As stated earlier, the basic idea in the two-layer formulation is to use the optimised configurations of Eq. (A22) as the basis functions for the complete wavefunction of the system $|\Phi\rangle$ which is

$$|\Phi\rangle = \sum_{n=1}^{N} A_n|\varphi_n\rangle e^{iS(\varphi_n)}. \quad \text{(A23)}$$

We shall once again employ the TDVP, this time taking only the amplitudes A_n as variational parameters, while using the previously individually optimised dynamics for the configurations $|\varphi_n\rangle$; the implicit assumption is that the single-configuration dynamics can be regarded as a good approximation for the dynamics that would result from a full variational approach.

As in the previous case, it is convenient to work with the Lagrangian L, defined as

$$L = i\langle\Phi|\dot{\Phi}\rangle - \langle\Phi|\hat{H}|\Phi\rangle \quad \text{(A24)}$$

and the alternative action functional in Eq. (A12), which includes a Lagrange multiplier to enforce normalisation. Here, the norm N reads

$$N = \langle\Phi|\Phi\rangle = \sum_{mn=1}^{N} A^*_n A_m\langle\varphi_n|\varphi_m\rangle e^{i(S(\varphi m) - S(\varphi_n))}, \quad \text{(A25)}$$

while L is explicitly given by the expression

$$L = \sum_{nm=1}^{N}\left[iA^*_n\dot{A}_m\langle\varphi_n|\varphi_m\rangle + A^*_n A_m\left(i\langle\varphi_n|\dot{\varphi}_m\rangle - \dot{S}_{\varphi_m}\langle\varphi_n|\varphi_m\rangle\right) - A^*_n A_m\langle\varphi_n|\hat{H}|\varphi_m\rangle\right] e^{i(S(\varphi_m) - S(\varphi_n))}. \quad \text{(A26)}$$

The formalism developed earlier applies here in the exact same manner; in the present context, Euler-Lagrange equation (A13b) translates to

$$\frac{\partial L}{\partial A^*_n} - (\lambda + L)\frac{\partial N}{\partial A^*_n} = 0 \quad \text{(A27)}$$

since L of Eq. (A26) does not depend on $\dot{A}^*_n$. The value of the multiplier can be obtained as before; this time, since A^*_n appears linearly in all the terms of L, we find

$$\lambda = \sum_{n=1}^{N} A^*_n\frac{\partial L}{\partial A^*_n} - L = 0, \quad \text{(A28)}$$

so that the equation for A reads

$$\sum_{m=1}^{N}\langle\varphi_n|\varphi_m\rangle(i\dot{A}_m - LA_m)e^{i(S(\varphi_m) - S(\varphi_n))} = \sum_{m=1}^{N}\left[\langle\varphi_n|\hat{H}|\varphi_m\rangle - i\langle\varphi_n|\dot{\varphi}_m\rangle + \dot{S}_m\langle\varphi_n|\varphi_m\rangle\right] A_m e^{i(S(\varphi_m) - S(\varphi_n))}. \quad \text{(A29)}$$

Defining new amplitudes D_m through the relation

$$A_m = D_m e^{-iS}, \quad \text{(A30)}$$

we are directly led to Eq. (19) of Sec. II, from where equations of motion (20) and (21) for D_n follows.

Finally, we write down the phase-corrected complete wavefunction $|\Psi\rangle = |\Phi\rangle e^{iS}$,

$$|\Psi\rangle = \sum_{n=1}^{N} D_n |\varphi_n\rangle e^{iS(\varphi_n)} \tag{A31a}$$

$$= \sum_{n=1}^{N} D_n \left[\sum_{k=1}^{K} d_{kn} |\mathbf{z}_{kn}^{(\mathrm{q})}\rangle e^{iS_{kn}^{(\mathrm{q})}}\right] |\mathbf{z}_n^{(\mathrm{c})}\rangle e^{i\theta_m^{(\mathrm{c})}} \tag{A31b}$$

$$= \sum_{n=1}^{N} D_n \sum_{k=1}^{K} d_{kn} |\mathbf{z}_{kn}\rangle e^{iS_{kn}} \tag{A31c}$$

which is exactly Eq. (9c) given in Section II [after substituting a_{kn} for d_{kn} in that equation, using Eq. (14)]. This completes the derivation of the working equations of the 2L-CCS method.

APPENDIX B: BENCHMARK CALCULATIONS

The wavefunction is represented as a basis set expansion

$$|\Psi(t)\rangle = \sum_{j=1}^{N_{\mathrm{bth}}} \sum_{n=1}^{N_{\mathrm{sys}}} c_{jn}(t) |\psi_j^{\mathrm{b}}\rangle |\psi_n^{\mathrm{s}}\rangle, \tag{B1}$$

in which $c_{jn}(t)$ are complex, time-dependent amplitudes, $|\psi_j^{\mathrm{b}}\rangle$ is a time-independent basis function for the bath modes, and $|\psi_n^{\mathrm{s}}\rangle$ is a time-independent basis function for the system mode. The number of bath and system basis functions is given by N_{bth} and N_{sys}, respectively. Substitution into the time-dependent Schrödinger equation leads to an equation for the time-dependence of the amplitudes

$$\frac{\mathrm{d}c_{im}(t)}{\mathrm{d}t} = -i \sum_{j=1}^{N_{\mathrm{bth}}} \sum_{n=1}^{N_{\mathrm{sys}}} H_{imjn} c_{jn}(t), \tag{B2}$$

where H_{imjn} is the Hamiltonian matrix

$$\begin{aligned} H_{imjn} &= \langle \psi_i^{\mathrm{b}} \psi_m^{\mathrm{s}} | \hat{H} | \psi_j^{\mathrm{b}} \psi_n^{\mathrm{s}} \rangle \\ &= \langle \psi_m^{\mathrm{s}} | \frac{\hat{p}^{(1)^2}}{2} - \frac{\hat{q}^{(1)^2}}{2} + \frac{\hat{q}^{(1)^4}}{16\xi} | \psi_n^{\mathrm{s}} \rangle \delta_{ij} \\ &\quad + \langle \psi_i^{\mathrm{b}} | \frac{\hat{\mathbf{P}}^2}{2} + \frac{\hat{\mathbf{Q}}^2}{2} | \psi_j^{\mathrm{b}} \rangle \delta_{mn} \\ &\quad + \frac{\lambda}{2} \langle \psi_i^{\mathrm{b}} | \hat{\mathbf{Q}}^2 | \psi_j^{\mathrm{b}} \rangle \langle \psi_m^{\mathrm{s}} | \hat{q}^{(1)} | \psi_n^{\mathrm{s}} \rangle. \end{aligned} \tag{B3}$$

The bath and system basis functions are orthonormal (see below), a fact that has been exploited in the above.

The bath modes are nearly harmonic; therefore, they can be represented by harmonic oscillator basis functions. A complete description of the bath would involve all excited state configurations; however, in practice, we can simply add on configurations until a converged result is achieved. For an $M-1$ dimensional bath, an excited state is comprised of the product of $M-1$ single particle harmonic oscillator functions, $\prod_{l=2}^{M} |\chi^{(l)}\rangle$, with different permutations of this product yielding different configurations. As the coupling of system and bath modes is proportional to $\hat{\mathbf{Q}}^2$ and all bath modes are initially in the ground state, only even excitations are involved. The size of the bath basis can be reduced further by exploiting the effective indistinguishability of the bath modes. The amplitudes of the harmonic oscillator excited state configurations, which correspond to similar vibrational excitations but differ only by the bath modes involved, will be identical for a given excited state. This means that configurations corresponding to the same excited state can be grouped together and associated with a single amplitude. This simplification reflects the permutational symmetry of the Hamiltonian in (22), as mentioned in Sec. III B. For example, if we include all even excitations up to a total quanta of 8, as used in the fully converged benchmark result for Hamiltonian (22), then the bath basis functions are

$$\begin{aligned} |\psi_1^{\mathrm{b}}\rangle &= |0000\ldots0000\rangle, \\ |\psi_2^{\mathrm{b}}\rangle &= (|2000\ldots0000\rangle + \cdots + |0000\ldots0002\rangle) \\ &\quad \times 1/\sqrt{M-1}, \\ |\psi_3^{\mathrm{b}}\rangle &= (|4000\ldots0000\rangle + \cdots + |0000\ldots0004\rangle) \\ &\quad \times 1/\sqrt{M-1}, \\ |\psi_4^{\mathrm{b}}\rangle &= (|2200\ldots0000\rangle + \cdots + |0000\ldots0022\rangle) \\ &\quad \times \sqrt{2!}/\sqrt{(M-1)(M-2)}, \\ |\psi_5^{\mathrm{b}}\rangle &= (|6000\ldots0000\rangle + \cdots + |0000\ldots0006\rangle) \\ &\quad \times 1/\sqrt{M-1}, \\ |\psi_6^{\mathrm{b}}\rangle &= (|4200\ldots0000\rangle + \cdots + |0000\ldots0024\rangle) \\ &\quad \times 1/\sqrt{(M-1)(M-2)}, \\ |\psi_7^{\mathrm{b}}\rangle &= (|2220\ldots0000\rangle + \cdots + |0000\ldots0222\rangle) \\ &\quad \times \sqrt{3!}/\sqrt{(M-1)(M-2)(M-3)}, \\ |\psi_8^{\mathrm{b}}\rangle &= (|8000\ldots0000\rangle + \cdots + |0000\ldots0008\rangle) \\ &\quad \times 1/\sqrt{M-1}, \\ |\psi_9^{\mathrm{b}}\rangle &= (|6200\ldots0000\rangle + \cdots + |0000\ldots0026\rangle) \\ &\quad \times 1/\sqrt{(M-1)(M-2)}, \\ |\psi_{10}^{\mathrm{b}}\rangle &= (|4400\ldots0000\rangle + \cdots + |0000\ldots0044\rangle) \\ &\quad \times \sqrt{2!}/\sqrt{(M-1)(M-2)}, \\ |\psi_{11}^{\mathrm{b}}\rangle &= (|4220\ldots0000\rangle + \cdots + |0000\ldots0224\rangle) \\ &\quad \times \sqrt{2!}/\sqrt{(M-1)(M-2)(M-3)}, \\ |\psi_{12}^{\mathrm{b}}\rangle &= (|2222\ldots0000\rangle + \cdots + |0000\ldots2222\rangle) \\ &\quad \times \sqrt{4!}/\sqrt{(M-1)(M-2)(M-3)(M-4)} \end{aligned} \tag{B4}$$

with relevant normalisation factors included. The square of the normalisation factors is simply equal to the number of configurations grouped; in this case, there are 8855 bath configurations governed by only 12 distinct amplitudes.

The basis functions for the system are those of a rectangular box

$$\langle q^{(1)} | \psi_n^{\mathrm{s}} \rangle = \sqrt{\frac{2}{L}} \sin\left(\frac{n\pi}{L}(q^{(1)} - q_{\mathrm{box}})\right), \tag{B5}$$

with L being the size of the box and q_{box} its left hand coordinate. Values of $L = 12$ and $q_{\mathrm{box}} = -6$ are used to enable a large enough area of coordinate space to be covered.

Now the basis functions have been defined, the matrix elements of the Hamiltonian may be evaluated. First, the bath elements

$$\langle \psi_i^{\mathrm{b}} | \frac{\hat{\mathbf{P}}^2}{2} + \frac{\hat{\mathbf{Q}}^2}{2} | \psi_j^{\mathrm{b}} \rangle = \delta_{ij} \left(E_i + \frac{M-1}{2}\right) \tag{B6}$$

are simply the harmonic oscillator eigenvalues for the excited states. The value of E_i is the sum of quanta in a particular excited state $E_i = \sum_{l=2}^{M} \epsilon_i^{(l)}$, where $\epsilon_i^{(l)}$ is the number of quanta in one mode. Second, the system elements

$$\langle \psi_m^{\mathrm{s}} | \frac{\hat{p}^{(1)^2}}{2} - \frac{\hat{q}^{(1)^2}}{2} + \frac{\hat{q}^{(1)^4}}{16\xi} | \psi_n^{\mathrm{s}} \rangle = \frac{n^2\pi^2}{2L^2}\delta_{mn} + \frac{2}{L}\int_{q_{\mathrm{box}}}^{q_{\mathrm{box}}+L} \sin\left(\frac{m\pi}{L}(q^{(1)} - q_{\mathrm{box}})\right) \sin\left(\frac{n\pi}{L}(q^{(1)} - q_{\mathrm{box}})\right) \left(\frac{\hat{q}^{(1)^4}}{16\xi} - \frac{\hat{q}^{(1)^2}}{2}\right) \mathrm{d}q^{(1)} \tag{B7}$$

are the particle in a box energy levels, plus an additional potential term. Finally, the system-bath interaction elements are given as

$$\langle \psi_i^{\mathrm{b}} | \hat{\mathbf{Q}}^2 | \psi_j^{\mathrm{b}} \rangle = \begin{cases} \frac{A_{ij}}{2}\sqrt{(\epsilon_i^{(l)} + 2)(\epsilon_i^{(l)} + 1)} & \text{if } \epsilon_i^{(l)} = \epsilon_j^{(l)} - 2 \text{ in only one mode and } \epsilon_i^{(l)} = \epsilon_j^{(l)} \text{ in all other modes} \\ \frac{A_{ij}}{2}\sqrt{\epsilon_i^{(l)}(\epsilon_i^{(l)} - 1)} & \text{if } \epsilon_i^{(l)} = \epsilon_j^{(l)} + 2 \text{ in only one mode and } \epsilon_i^{(l)} = \epsilon_j^{(l)} \text{ in all other modes} \\ \sum_{l=2}^{M} \epsilon_i^{(l)} + \frac{M-1}{2} & \text{if } \epsilon_i^{(l)} = \epsilon_j^{(l)} \text{ in all modes} \\ 0 & \text{if states differ by more than two quanta in one mode, or two quanta in more than one mode} \end{cases}, \tag{B8}$$

$$\langle \psi_m^{\mathrm{s}} | \hat{q}^{(1)} | \psi_n^{\mathrm{s}} \rangle = \frac{2}{L}\int_{q_{\mathrm{box}}}^{q_{\mathrm{box}}+L} \sin\left(\frac{m\pi}{L}(q^{(1)} - q_{\mathrm{box}})\right) \sin\left(\frac{n\pi}{L}(q^{(1)} - q_{\mathrm{box}})\right) q^{(1)}\,\mathrm{d}q^{(1)}, \tag{B9}$$

where A_{ij} is a constant that depends upon the normalisation factors and the number of configurations that differ by only two quanta in one mode between states. For clarity, the $\langle \psi_i^{\mathrm{b}} | \hat{\mathbf{Q}}^2 | \psi_j^{\mathrm{b}} \rangle$ matrix elements evaluated using the bath basis functions of Eq. (B4) are

$$\begin{array}{c} \\ \langle\psi_1^{\mathrm{b}}| \\ \langle\psi_2^{\mathrm{b}}| \\ \langle\psi_3^{\mathrm{b}}| \\ \langle\psi_4^{\mathrm{b}}| \\ \langle\psi_5^{\mathrm{b}}| \\ \langle\psi_6^{\mathrm{b}}| \\ \langle\psi_7^{\mathrm{b}}| \\ \langle\psi_8^{\mathrm{b}}| \\ \langle\psi_9^{\mathrm{b}}| \\ \langle\psi_{10}^{\mathrm{b}}| \\ \langle\psi_{11}^{\mathrm{b}}| \\ \langle\psi_{12}^{\mathrm{b}}| \end{array} \begin{array}{c} \begin{array}{cccccccccccc} |\psi_1^{\mathrm{b}}\rangle & |\psi_2^{\mathrm{b}}\rangle & |\psi_3^{\mathrm{b}}\rangle & |\psi_4^{\mathrm{b}}\rangle & |\psi_5^{\mathrm{b}}\rangle & |\psi_6^{\mathrm{b}}\rangle & |\psi_7^{\mathrm{b}}\rangle & |\psi_8^{\mathrm{b}}\rangle & |\psi_9^{\mathrm{b}}\rangle & |\psi_{10}^{\mathrm{b}}\rangle & |\psi_{11}^{\mathrm{b}}\rangle & |\psi_{12}^{\mathrm{b}}\rangle \end{array} \\ \begin{pmatrix} \frac{M-1}{2} & \frac{\sqrt{2(M-1)}}{2} & 0 & 0 & 0 & 0 & 0 & 0 & 0 & 0 & 0 & 0 \\ \frac{\sqrt{2(M-1)}}{2} & 2+\frac{M-1}{2} & \sqrt{3} & \sqrt{M-2} & 0 & 0 & 0 & 0 & 0 & 0 & 0 & 0 \\ 0 & \sqrt{3} & 4+\frac{M-1}{2} & 0 & \frac{1}{2}\sqrt{30} & \frac{\sqrt{2(M-2)}}{2} & 0 & 0 & 0 & 0 & 0 & 0 \\ 0 & \sqrt{M-2} & 0 & 4+\frac{M-1}{2} & 0 & \sqrt{6} & \frac{\sqrt{6(M-3)}}{2} & 0 & 0 & 0 & 0 & 0 \\ 0 & 0 & \frac{1}{2}\sqrt{30} & 0 & 6+\frac{M-1}{2} & 0 & 0 & \frac{1}{2}\sqrt{56} & \frac{\sqrt{2(M-2)}}{2} & 0 & 0 & 0 \\ 0 & 0 & \frac{\sqrt{2(M-2)}}{2} & \sqrt{6} & 0 & 6+\frac{M-1}{2} & 0 & 0 & \frac{1}{2}\sqrt{30} & \frac{1}{2}\sqrt{24} & \sqrt{M-3} & 0 \\ 0 & 0 & 0 & \frac{\sqrt{6(M-3)}}{2} & 0 & 0 & 6+\frac{M-1}{2} & 0 & 0 & 0 & \frac{1}{2}\sqrt{36} & \sqrt{2(M-4)} \\ 0 & 0 & 0 & 0 & \frac{1}{2}\sqrt{56} & 0 & 0 & 8+\frac{M-1}{2} & 0 & 0 & 0 & 0 \\ 0 & 0 & 0 & 0 & \frac{\sqrt{2(M-2)}}{2} & \frac{1}{2}\sqrt{30} & 0 & 0 & 8+\frac{M-1}{2} & 0 & 0 & 0 \\ 0 & 0 & 0 & 0 & 0 & \frac{1}{2}\sqrt{24} & 0 & 0 & 0 & 8+\frac{M-1}{2} & 0 & 0 \\ 0 & 0 & 0 & 0 & 0 & \sqrt{M-3} & \frac{1}{2}\sqrt{36} & 0 & 0 & 0 & 8+\frac{M-1}{2} & 0 \\ 0 & 0 & 0 & 0 & 0 & 0 & \sqrt{2(M-4)} & 0 & 0 & 0 & 0 & 8+\frac{M-1}{2} \end{pmatrix} \end{array}. \tag{B10}$$

The initial amplitudes are calculated via projection onto the initial wavepacket, with all modes in the ground vibrational level at $t = 0$,

$$\begin{aligned} c_{im}(0) &= \langle \psi_i^{\mathrm{b}} \psi_m^{\mathrm{s}} | \Psi(0) \rangle = \delta_{1m} \langle \psi_m^{\mathrm{s}} | \Psi(0) \rangle \\ &= \sqrt{\frac{2}{L}} \int_{q_{\mathrm{box}}}^{q_{\mathrm{box}}+L} \sin\left(\frac{m\pi}{L}(q^{(1)} - q_{\mathrm{box}})\right) \\ &\quad \times \left(\frac{1}{\pi}\right)^{\frac{1}{4}} \exp\left(-\frac{1}{2}\left(q^{(1)} - q^{(1)}(0)\right)^2\right) \mathrm{d}q^{(1)}. \end{aligned} \tag{B11}$$

The CCF is calculated via the overlap between the wavefunction and the mirror image of the initial state,

$$\begin{aligned} \mathrm{CCF}(t) &= \langle \bar{\Psi}(0) | \Psi(t) \rangle \\ &= \sum_{i,j=1}^{N_{\mathrm{bth}}} \sum_{m,n=1}^{N_{\mathrm{sys}}} \bar{c}_{im}^*(0) c_{jn}(t) \langle \psi_i^{\mathrm{b}} \psi_m^{\mathrm{s}} | \psi_j^{\mathrm{b}} \psi_n^{\mathrm{s}} \rangle \\ &= \sum_{i,j=1}^{N_{\mathrm{bth}}} \sum_{m,n=1}^{N_{\mathrm{sys}}} \bar{c}_{im}^*(0) c_{jn}(t) \delta_{ij} \delta_{mn} \\ &= \sum_{j=1}^{N_{\mathrm{bth}}} \sum_{n=1}^{N_{\mathrm{sys}}} \bar{c}_{jn}^*(0) c_{jn}(t), \end{aligned} \tag{B12}$$

where the mirror image of the initial state has been expressed as the basis set expansion with coefficients $\bar{c}_{jn}$, and the orthogonality of the basis functions has been utilised.

The benchmark is converged with respect to N_{bth} and N_{sys}, with fully converged values of $N_{\text{bth}} = 12$ (number of basis functions to give even harmonic oscillator excited states up to a quanta of 8) and $N_{\text{sys}} = 50$.

[1]H.-D. Meyer, U. Manthe, and L. S. Cederbaum, Chem. Phys. Lett. **165**, 73 (1990).
[2]C. Lubich, *From Quantum to Classical Molecular Dynamics: Reduced Models and Numerical Analysis*, Zurich Lectures in Advanced Mathematics (European Mathematical Society (EMS), 2008).
[3]H. Wang and M. Thoss, J. Chem. Phys. **119**, 1289 (2003).
[4]U. Manthe, J. Chem. Phys. **128**, 164116 (2008).
[5]O. Vendrell and H.-D. Meyer, J. Chem. Phys. **134**, 044135 (2011).
[6]S. Römer, M. Ruckenbauer, and I. Burghardt, J. Chem. Phys. **138**, 064106 (2013).
[7]E. J. Heller, J. Chem. Phys. **75**, 2923 (1981).
[8]D. V. Shalashilin and M. S. Child, J. Chem. Phys. **113**, 10028 (2000).
[9]M. F. Herman and E. Kluk, Chem. Phys. **91**, 27 (1984).
[10]E. Kluk, M. F. Herman, and H. L. Davis, J. Chem. Phys. **84**, 326 (1986).
[11]K. G. Kay, Chem. Phys. **322**, 3 (2006).
[12]T. J. Martinez, M. Ben-Nun, and G. Ashkenazi, J. Chem. Phys. **104**, 2847 (1996).
[13]M. Ben-Nun and T. J. Martínez, Adv. Chem. Phys. **121**, 439 (2002).
[14]D. V. Shalashilin and M. S. Child, J. Chem. Phys. **115**, 5367 (2001).
[15]D. V. Shalashilin and M. S. Child, Chem. Phys. **304**, 103 (2004).
[16]D. V. Shalashilin and M. S. Child, J. Chem. Phys. **128**, 054102 (2008).
[17]G. A. Worth and I. Burghardt, Chem. Phys. Lett. **368**, 502 (2003).
[18]D. V. Shalashilin and I. Burghardt, J. Chem. Phys. **129**, 084104 (2008).
[19]D. V. Shalashilin, J. Chem. Phys. **130**, 244101 (2009).
[20]D. V. Shalashilin, J. Chem. Phys. **132**, 244111 (2010).
[21]D. V. Shalashilin, Faraday Discuss. **153**, 105 (2011).
[22]S.-Y. Ye, D. Shalashilin, and A. Serafini, Phys. Rev. A **86**, 032312 (2012).
[23]I. Burghardt, H.-D. Meyer, and L. S. Cederbaum, J. Chem. Phys. **111**, 2927 (1999).
[24]S. K. Reed, M. L. González-Martínez, J. Rubayo-Soneira, and D. V. Shalashilin, J. Chem. Phys. **134**, 054110 (2011).
[25]K. Saita and D. V. Shalashilin, J. Chem. Phys. **137**, 22A506 (2012).
[26]K. Saita, M. G. D. Nix, and D. V. Shalashilin, Phys. Chem. Chem. Phys. **15**, 16227 (2013).
[27]D. V. Makhov, W. J. Glover, T. J. Martinez, and D. V. Shalashilin, J. Chem. Phys. **141**, 054110 (2014).
[28]D. V. Makhov, K. Saita, T. J. Martinez, and D. V. Shalashilin, Phys. Chem. Chem. Phys. **17**, 3316 (2015).
[29]G. D. Billing, J. Chem. Phys. **65**, 1 (1976).
[30]G. D. Billing, Chem. Phys. Lett. **100**, 535 (1983).
[31]G. D. Billing, *The Quantum Classical Theory* (Oxford University Press, Oxford, NY, 2003).
[32]J. R. Klauder and B. S. Skagerstam, *Coherent States: Applications in Physics and Mathematical Physics* (World Scientific, Singapore, 1985).
[33]S. Römer and I. Burghardt, Mol. Phys. **111**, 3618 (2013).
[34]M. Ronto and D. V. Shalashilin, J. Phys. Chem. A **117**, 6948 (2013).
[35]Y. Wu and V. S. Batista, J. Chem. Phys. **121**, 1676 (2004).
[36]P. A. Sherratt, D. V. Shalashillin, and M. S. Child, Chem. Phys. **322**, 127 (2006).
[37]S. Habershon, J. Chem. Phys. **136**, 054109 (2012).
[38]J. A. Green and D. V. Shalashilin, Chem. Phys. Lett. **641**, 173 (2015).
[39]D. V. Shalashilin, M. S. Child, and D. C. Clary, J. Chem. Phys. **120**, 5608 (2004).
[40]C. Symonds, J. Wu, M. Ronto, C. Zagoya, C. Figueira de Morisson Faria, and D. V. Shalashilin, Phys. Rev. A **91**, 023427 (2015).
[41]P. Kramer and M. Saraceno, *Geometry of the Time-Dependent Variational Principle in Quantum Mechanics*, Lecture Notes in Physics Vol. 140 (Springer, Berlin, Heidelberg, 1981).

[42]We assume real parameters for simplicity, but, of course, this also accounts for complex parametrisations: One can always work separately with real and imaginary parts or, alternatively, treat the parameters and their complex conjugates as independent variabless – both approaches are equivalent.
[43]In order to come to this conclusion one must consider the case of unrestricted variations and work out the Euler-Lagrange equations of motion; the resulting equation coincides with the Schrödinger equation except for a time-dependent phase; both normalisation factor and action phase are introduced precisely to cancel this factor.
[44]The coefficients b_{kn} in Eq. (A7) differ from the coefficients a_{kn} of Eq. (8) by a time-dependent phase – see Eq. (14).